ELSEVIER

Comput. Methods Appl. Mech. Engrg. 190 (2001) 6023–6052

Computer methods in applied mechanics and engineering

www.elsevier.com/locate/cma

Co-rotational formulation for geometric nonlinear analysis of doubly symmetric thin-walled beams

Wen Yi Lin [a], Kuo Mo Hsiao [b,*]

[a] *Department of Mechanical Engineering, Der Lin Institute of Technology, 1 Alley 380, Ching Yun Road, Tucheng, Taiwan, ROC*
[b] *Department of Mechanical Engineering, National Chiao Tung University, 1001 Ta Hsueh Road, Hsinchu, Taiwan, ROC*

Received 24 December 1999; received in revised form 14 September 2000

Abstract

A doubly symmetric thin-walled beam element with open section is derived using co-rotational (CR) total Lagrangian (TL) formulation. The effects of deformation-dependent third-order terms of element nodal forces on the buckling load and post-buckling behavior are investigated. All coupling among bending, twisting, and stretching deformations for beam element is considered by consistent second-order linearization of the fully geometrically nonlinear beam theory. However, all third-order terms of nodal forces, which are relevant to the twist rate, rate of twist rate and curvature of the beam axis are also considered. An incremental-iterative method based on the Newton–Raphson method combined with constant arc length of incremental displacement vector is employed for the solution of nonlinear equilibrium equations. The zero value of the tangent stiffness matrix determinant of the structure is used as the criterion of the buckling state. A parabolic interpolation method of the arc length is used to find the buckling load. Numerical examples are presented to demonstrate the accuracy and efficiency of the proposed element and to investigate the effect of third-order terms of element nodal forces on the buckling load and post-buckling behavior of doubly symmetric thin-walled beams.

Keywords: Co-rotational formulation; Thin-walled beam; Geometric nonlinearity; Buckling; Postbuckling

1. Introduction

Due to reduction of weight, material and cost, thin-walled beams with open section are extensively used in aerospace and aircraft structures, and are often designed to work under post-buckling conditions. Such flexible structures can undergo large displacements and rotations without exceeding their elastic limits. To understand the behaviors of such flexible structures and to evaluate their elastic limits many different formulations and numerical procedures for the buckling and post-buckling analysis of thin-walled beams have been proposed [1–35]. The buckling of the beam structures is caused by the coupling among bending, twisting, and stretching deformations of the beam members. Thus the buckling analysis is a subtopic of nonlinear rather than linear mechanics [7]. Currently, the most popular approach for the analysis of three-dimensional beam is to develop finite element models. The formulations, which have been used in the literature, might be divided into three categories: total Langrangian (TL) formulation, updated Lagrangian (UL) formulation, and co-rotational (CR) formulation. In order to capture correctly all coupling among bending, twisting, and stretching deformations of the beam elements, the formulation of beam elements might be derived by the fully geometrically nonlinear beam theory [36]. The exact expressions for the element nodal forces, which are required in a TL formulation for large displacement/small strain problems,

* Corresponding author. Fax: +886-35-720-634.
E-mail address: kmhsiao@cc.nctu.edu.tw (K.M. Hsiao).

0045-7825/01/$ - see front matter
PII: S0045-7825(01)00212-2

are highly nonlinear functions of element nodal parameters. However, the dominant factors in the geometrical nonlinearities of beam structures are attributable to finite rotations, the strains remaining small. For a beam structure discretized by finite elements, this implies that the motion of the individual elements to a large extent will consist of rigid body motion. If the rigid body motion part is eliminated from the total displacements and the element size is properly chosen, the deformational part of the motion is always small relative to the local element axes. Thus in conjunction with the CR formulation, the higher-order terms of nodal parameters in the element nodal forces may be neglected by consistent second-order linearization [32,36]. However, the values of twist rate, the rate of twist rate and curvature of the beam axis are deformation dependent, not element size dependent. Thus their values may not always be much smaller than unity. It seems that some third-order terms of the element nodal forces, which are relevant to the twist rate, the rate of twist rate and curvature of the beam axis, may not be negligible for some cross-sections with large rotations. In [34], the effect of these deformation-dependent third-order terms of element nodal forces on the buckling load and post-buckling behavior was investigated for doubly symmetric beams with solid sections. It was reported in [34] that the third-order term of twist rate is the dominant third-order term of the element nodal forces and may not be negligible for the buckling and post-buckling analysis. In [35] the formulation proposed in [32] for beams with solid sections was extended to the thin-walled beam with monosymmetric open section. In [35] the third-order term of the twist rate is considered in element nodal forces. However, the effect of deformation-dependent third-order terms of element nodal forces on the buckling load and post-buckling behavior was not investigated in [35]. To the authors' knowledge, the effect of deformation-dependent third-order terms of element nodal forces on the buckling load and post-buckling behavior of thin-walled beam with open section has not been reported in the literature.

The doubly symmetric thin-walled beam has been extensively used in practice. Thus, a reliable and efficient formulation for geometric nonlinear analysis of doubly symmetrical thin-walled beam may be required. The object of this paper is to present a CR TL finite element formulation for the geometric nonlinear analysis of doubly symmetrical thin-walled beams and to investigate the effects of deformation-dependent third-order terms of element nodal forces on the buckling load and post-buckling behavior of thin-walled beam.

The shear center and centroid are coincident for doubly symmetric beam but not for monosymmetric beam. Thus, the kinematics of the monosymmetric beam element is much more complicated than that of doubly symmetric beam element. The monosymmetric beam element proposed in [35] may be inefficient for the analysis of doubly symmetric beams. Moreover, the beam element proposed in [35] cannot be used to investigate the effect of third-order terms on the buckling load and post-buckling behavior of thin-walled beam. However, even beam elements proposed in [34,35] are not suitable for the present study, it seems that the formulations given in [34,35] can be adapted for doubly symmetric thin-walled beams. Thus, the formulations of beam elements proposed in [34,35] are modified and employed here. All third-order terms of the element nodal forces, which are relevant to the twist rate, the rate of twist rate and curvature of the beam axis, are retained here.

An incremental-iterative method based on the Newton–Raphson method combined with constant arc length of incremental displacement vector is employed for the solution of nonlinear equilibrium equations. The zero value of the tangent stiffness matrix determinant of the structure is used as the criterion of the buckling state. A parabolic interpolation method of the arc length is used to find the buckling load. An inverse power method for the solution of the generalized eigenvalue problem is used to find the corresponding buckling mode. In order to initiate the secondary path, at the bifurcation point a perturbation displacement proportional to the first buckling mode is added. Numerical examples are presented to demonstrate the accuracy and efficiency of the proposed method and to investigate the effect of third-order terms of the element nodal forces on the buckling load and post-buckling behavior of doubly symmetric thin-walled beams.

2. Finite element formulation

The formulations given in [34,35] are modified and employed here.

2.1. Basic assumptions

The following assumptions are made in the derivation of the beam element behavior.

1. The beam is prismatic and slender, and the Euler–Bernoulli hypothesis is valid.
2. The cross-section of the beam is doubly symmetric.
3. The unit extension of the centroid axis of the beam element is uniform.
4. The cross-section of the beam element does not deform in its own plane and strains within this cross-section can be neglected.
5. The out-of-plane warping of the cross-section is the product of the twist rate of the beam element and the Saint Venant warping function for a prismatic thin-walled beam of the same cross-section.
6. The deformation displacements of the beam element are small.

In this study, Prandtl's membrane analogy and the Saint Venant torsion theory [37] are used to obtain an approximate Saint Venant warping function for a prismatic thin-walled beam.

2.2. Coordinate systems

In this paper, a CR TL formulation is adopted. In order to describe the system, we define four sets of right-handed rectangular Cartesian coordinate systems:

1. *A fixed global set of coordinates*, X_i^G $(i = 1, 2, 3)$ (see Fig. 1); the nodal coordinates, displacements, and rotations, and the stiffness matrix of the system are defined in these coordinates.
2. *Element cross-section coordinates*, x_i^S $(i = 1, 2, 3)$ (see Fig. 1); a set of element cross-section coordinates is associated with each cross-section of the beam element. The origin of this coordinate system is rigidly tied to the shear center of the cross-section. The x_1^S axis is chosen to coincide with the normal of the unwarped cross-section and the x_2^S and x_3^S axes are chosen to be the principal directions of the cross-section.
3. *Element coordinates*; x_i $(i = 1, 2, 3)$ (see Fig. 1), a set of element coordinates is associated with each element, which is constructed at the current configuration of the beam element. The origin of this coordinate system is located at node 1, and the x_1 axis is chosen to pass through two shear centers of end sections of the element; the x_2 and x_3 axes are chosen to be the principal directions of the cross-section in the undeformed state. Note that this coordinate system is a local coordinate system not a moving coordinate system. The deformations, internal nodal forces and stiffness matrix of the elements are defined

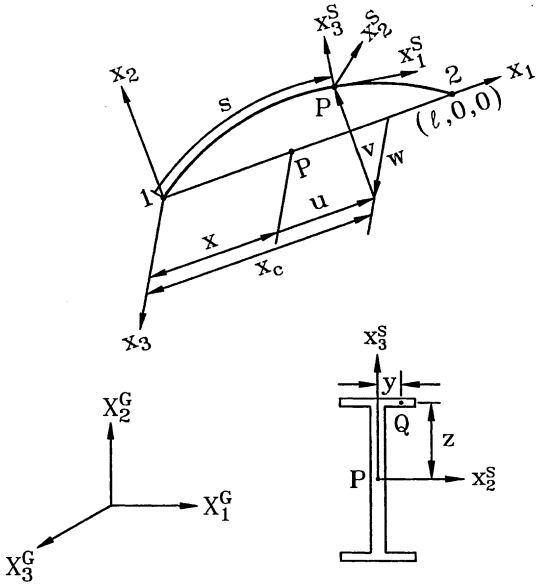

Fig. 1. Coordinate systems.

in terms of these coordinates. In this paper the element deformations are determined by the rotation of element cross-section coordinate systems relative to this coordinate system.

4. *Load base coordinates*, X_i^P $(i = 1, 2, 3)$; a set of load base coordinates is associated with each configuration-dependent moment. The origin of this coordinate system is chosen to be the node where the configuration-dependent moment is applied. The mechanism for generating configuration dependent moment is described in these coordinates, and the corresponding external load and load stiffness matrix are defined in terms of these coordinates.

In this paper, the symbol { } denotes the column matrix. The relations among the global coordinates, element cross-section coordinates, element coordinates and load base coordinates may be expressed by

$$\mathbf{X}^G = \mathbf{A}_{GS}\mathbf{x}^S, \quad \mathbf{X}^G = \mathbf{A}_{GE}\mathbf{x}, \quad \mathbf{X}^G = \mathbf{A}_{GP}\mathbf{X}^P, \tag{1}$$

where $\mathbf{X}^G = \{X_1^G, X_2^G, X_3^G\}$, $\mathbf{x}^S = \{x_1^S, x_2^S, x_3^S\}$, $\mathbf{x} = \{x_1, x_2, x_3\}$, and $\mathbf{X}^P = \{X_1^P, X_2^P, X_3^P\}$; $\mathbf{A}_{GS}$, $\mathbf{A}_{GE}$, and $\mathbf{A}_{GP}$ are the matrices of direction cosines of the element cross-section coordinate system, element coordinate system, and load base coordinate system, respectively.

2.3. Rotation vector

For the convenience of later discussion, the term 'rotation vector' is used to represent a finite rotation. Fig. 2 shows that a vector $\mathbf{b}$ which as a result of the application of a rotation vector $\phi\mathbf{a}$ is transported to the new position $\bar{\mathbf{b}}$. The relation between $\bar{\mathbf{b}}$ and $\mathbf{b}$ may be expressed as [38]

$$\bar{\mathbf{b}} = \cos\phi\mathbf{b} + (1 - \cos\phi)(\mathbf{a}\cdot\mathbf{b})\mathbf{a} + \sin\phi(\mathbf{a}\times\mathbf{b}), \tag{2}$$

where ϕ is the angle of counterclockwise rotation, and $\mathbf{a}$ is the unit vector along the axis of rotation.

2.4. Kinematics of beam element

The deformations of the beam element are described in the current element coordinate system. From the kinematic assumptions made in this paper, the deformations of the beam element may be determined by the displacements of the shear center axis of the beam element, orientation of the cross-section (element cross-section coordinates), and the out-of-plane warping of the cross-section. In this study only the doubly symmetric cross-section is considered. Thus the shear center and centroid of the cross-section are coincident. Let Q (Fig. 1) be an arbitrary point in the beam element, and P be the point corresponding to Q on

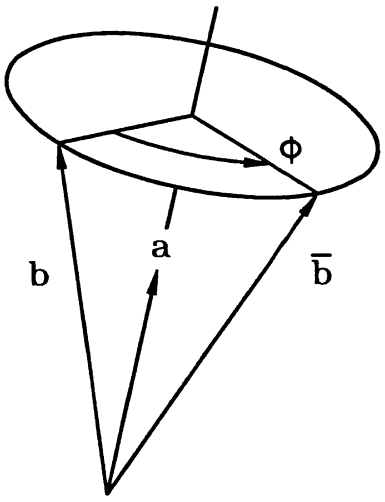

Fig. 2. Rotation vector.

the shear center axis. The position vector of point Q in the undeformed and deformed configurations may be expressed as

$$\mathbf{r}_0 = x\mathbf{e}_1 + y\mathbf{e}_2 + z\mathbf{e}_3 \tag{3}$$

and

$$\mathbf{r} = x_c(x)\mathbf{e}_1 + v(x)\mathbf{e}_2 + w(x)\mathbf{e}_3 + \theta_{1,x}\omega\mathbf{e}_1^S + y\mathbf{e}_2^S + z\mathbf{e}_3^S, \tag{4}$$

where $x_c(x), v(x)$, and $w(x)$ are the x_1, x_2 and x_3 coordinates of point P, respectively, in the deformed configuration, $\omega = \omega(y,z)$ is the Saint Venant warping function for a prismatic beam of the same cross-section, and $\mathbf{e}_i$ and $\mathbf{e}_i^S$ $(i = 1,2,3)$ denote the unit vectors associated with the x_i and x_i^S axes, respectively. Note that $\mathbf{e}_i$ and $\mathbf{e}_i^S$ are coincident in the undeformed state. Here, the triad $\mathbf{e}_i^S$ in the deformed state is assumed to be achieved by the successive application of the following two rotation vectors to the triad $\mathbf{e}_i$:

$$\boldsymbol{\theta}_n = \theta_n\mathbf{n} \tag{5}$$

and

$$\boldsymbol{\theta}_t = \theta_1\mathbf{t}, \tag{6}$$

where

$$\mathbf{n} = \{0, \theta_2/(\theta_2^2+\theta_3^2)^{1/2}, \theta_3/(\theta_2^2+\theta_3^2)^{1/2}\}, \tag{7}$$

$$\mathbf{t} = \{\cos\theta_n,\ \theta_3,\ -\theta_2\}, \tag{8}$$

$$\cos\theta_n = (1-\theta_2^2-\theta_3^2)^{1/2}, \tag{9}$$

$$\theta_2 = -\frac{\mathrm{d}w(x)}{\mathrm{d}s} = -\frac{\mathrm{d}w(x)}{\mathrm{d}x}\frac{\mathrm{d}x}{\mathrm{d}s} = -\frac{w'}{1+\varepsilon_c}, \tag{10}$$

$$\theta_3 = \frac{\mathrm{d}v(x)}{\mathrm{d}s} = \frac{\mathrm{d}v(x)}{\mathrm{d}x}\frac{\mathrm{d}x}{\mathrm{d}s} = \frac{v'}{1+\varepsilon_c}, \tag{11}$$

$$\varepsilon_c = \frac{\partial s}{\partial x} - 1, \tag{12}$$

in which $\mathbf{n}$ is the unit vector perpendicular to the vectors $\mathbf{e}_1$ and $\mathbf{e}_1^S$, and $\mathbf{t}$ is the tangent unit vector of the deformed shear center axis of the beam element. Note that the orientation of $\mathbf{e}_1^S$ coincides with that of $\mathbf{t}$. θ_1 is the rotation about vector $\mathbf{t}$. θ_n is the angle measured from x_1 axis to vector $\mathbf{t}$, ε_c is the unit extension of the shear center axis and s is the arc length of the deformed shear center axis measured from node 1 to point P. In this paper, the symbol $(\,)'$ denotes $(\,)_{,x} = \partial(\,)/\partial x$.

Using Eqs. (2)–(8), the relation between the vectors $\mathbf{e}_i$ and $\mathbf{e}_i^S$ $(i = 1,2,3)$ in the element coordinate system may be obtained as [32]

$$\mathbf{e}_i^S = \mathbf{R}\mathbf{e}_i, \tag{13}$$

where $\mathbf{R}$ is the so-called rotation matrix. The rotation matrix is determined by θ_i $(i = 1,2,3)$. Thus, θ_i are called the rotation parameters in this study.

Let $\boldsymbol{\theta} = \{\theta_1, \theta_2, \theta_3\}$ be the column matrix of rotation parameters, $\delta\boldsymbol{\theta}$ be the variation of $\boldsymbol{\theta}$. The triad $\mathbf{e}_i^S$ $(i = 1,2,3)$ corresponding to $\boldsymbol{\theta}$ may be rotated by a rotation vector $\delta\boldsymbol{\phi} = \{\delta\phi_1, \delta\phi_2, \delta\phi_3\}$ to reach their new positions corresponding to $\boldsymbol{\theta} + \delta\boldsymbol{\theta}$ [32]. When θ_2 and θ_3 are much smaller than unity, the relationship between $\delta\boldsymbol{\theta}$ and $\delta\boldsymbol{\phi}$ may be approximated by [32]

$$\delta\boldsymbol{\theta} = \begin{bmatrix} 1 & \theta_3/2 & -\theta_2/2 \\ -\theta_3 & 1 & 0 \\ \theta_2 & 0 & 1 \end{bmatrix} \delta\boldsymbol{\phi} = \mathbf{T}^{-1}\delta\boldsymbol{\phi}. \tag{14}$$

The relationship among $x_c(x), v(x), w(x)$, and x may be given as

$$x_c(x) = u_1 + \int_0^x [(1+\varepsilon_c)^2 - v_{,x}^2 - w_{,x}^2]^{1/2}\,\mathrm{d}x, \tag{15}$$

where u_1 is the displacement of node 1 in the x_1 direction. Note that due to the definition of the element coordinate system, the value of u_1 is equal to zero. However, the variation of u_1 is not zero. Making use of Eq. (15), one obtains

$$\ell = L + u_2 - u_1 = x_c(L) - x_c(0) = \int_0^L [(1+\varepsilon_c)^2 - v_{,x}^2 - w_{,x}^2]^{1/2}\,\mathrm{d}x, \tag{16}$$

in which ℓ is the current chord length of the shear center axis of the beam element, and L is the length of the undeformed beam axis, and u_2 is the displacement of node 2 in the x_1 direction. Making use of the assumption of uniform unit extension, ε_c may be calculated using Eq. (16).

Here, the lateral deflections of the shear center axis, $v(x)$ and $w(x)$, and the rotation about the shear center axis, $\theta_1(x)$, are assumed to be the Hermitian polynomials of x. $v(x), w(x)$ and $\theta_1(x)$ may be expressed by

$$\begin{aligned} v(x) &= \{N_1, N_2, N_3, N_4\}^t\{v_1, v_1', v_2, v_2'\} = \mathbf{N}_b^t\mathbf{u}_b, \\ w(x) &= \{N_1, -N_2, N_3, -N_4\}^t\{w_1, -w_1', w_2, -w_2'\} = \mathbf{N}_c^t\mathbf{u}_c, \\ \theta_1(x) &= \{N_1, N_2, N_3, N_4\}^t\{\theta_{11}, \beta_1, \theta_{12}, \beta_2\} = \mathbf{N}_d^t\mathbf{u}_d, \end{aligned} \tag{17}$$

where v_j and w_j $(j = 1, 2, 3)$ are the nodal values of v and w at nodes j, respectively, v_j' and w_j' $(j = 1, 2)$ are the nodal values of $v_{,x}$ and $w_{,x}$ at nodes j, respectively, and θ_{1j} and β_j $(j = 1, 2)$ are nodal values of θ_1, $\theta_{1,x}$ at nodes j, respectively. Note that, due to the definition of the element coordinates, the values of v_j and w_j $(j = 1, 2)$ are zero. However, their variations are not zero. N_i $(i = 1$–$4)$ are the shape functions and are given by

$$\begin{aligned} N_1 &= \frac{1}{4}(1-\xi)^2(2+\xi), \quad N_2 = \frac{L}{8}(1-\xi^2)(1-\xi), \\ N_3 &= \frac{1}{4}(1+\xi)^2(2-\xi), \quad N_4 = \frac{L}{8}(-1+\xi^2)(1+\xi), \end{aligned} \tag{18}$$

where

$$\xi = -1 + \frac{2x}{L}. \tag{19}$$

The axial displacements of the shear center axis may be determined from the lateral deflections and the unit extension of the shear center axis using Eq. (15).

If x, y and z in Eq. (3) are regarded as the Lagrangian coordinates, the Green strain $\varepsilon_{11}, \varepsilon_{12}$ and ε_{13} are given by [39]

$$\varepsilon_{11} = \frac{1}{2}(\mathbf{r}_{,x}^t\mathbf{r}_{,x} - 1), \quad \varepsilon_{12} = \frac{1}{2}\mathbf{r}_{,x}^t\mathbf{r}_{,y}, \quad \varepsilon_{13} = \frac{1}{2}\mathbf{r}_{,x}^t\mathbf{r}_{,z}. \tag{20}$$

Substituting Eqs. (4), (8)–(13) into Eq. (20) and retaining all terms up to the second-order and the third-order terms, which are relevant to the retained third-order terms of nodal forces, yield

$$\varepsilon_{11} = \varepsilon_c - yv_{,xx} - zw_{,xx} + \omega\theta_{1,xx} + \frac{1}{2}\varepsilon_c^2 + \omega\varepsilon_c\theta_{1,xx} + \frac{1}{2}(y^2+z^2)\theta_{1,x}^2 + \frac{1}{2}v_{,xx}^2 + \frac{1}{2}z^2w_{,xx}^2 + \frac{1}{2}\omega^2\theta_{1,xx}^2 - y\theta_1 w_{,xx} + z\theta_1 v_{,xx} + yzv_{,xx}w_{,xx} - y\omega v_{,xx}\theta_{1,xx} - z\omega w_{,xx}\theta_{1,xx} \underline{- y\omega\theta_{1,x}^2 w_{,xx} - z\omega\theta_{1,x}^2 v_{,xx}}, \tag{21}$$

$$\varepsilon_{12} = \frac{1}{2}(\omega_{,y} - z)\theta_{1,x} + \frac{1}{4}z(v_{,x}w_{,xx} - w_{,x}v_{,xx}) + \frac{1}{2}\left[\omega_{,y}\varepsilon_c\theta_{1,x} + (\omega - y\omega_{,y})\theta_{1,x}v_{,xx} - z\omega_{,y}\theta_{1,x}w_{,xx} + \omega\omega_{,y}\theta_{1,x}\theta_{1,xx}\right], \tag{22}$$

$$\varepsilon_{13} = \frac{1}{2}(\omega_{,z} + y)\theta_{1,x} + \frac{1}{4}y(w_{,x}v_{,xx} - v_{,x}w_{,xx}) + \frac{1}{2}[\omega_{,z}\varepsilon_c\theta_{1,x} + (\omega - z\omega_{,z})\theta_{1,x}w_{,xx} - y\omega_{,z}\theta_{1,x}v_{,xx} + \omega\omega_{,z}\theta_{1,x}\theta_{1,xx}]. \tag{23}$$

The underlined terms in Eq. (21) are the retained third-order terms of strains.

2.5. Nodal parameters and forces

The element employed here has two nodes with seven degrees of freedom per node. Two sets of element nodal parameters termed 'explicit nodal parameters' and 'implicit nodal parameters' are employed. The explicit nodal parameters of the element are used for the assembly of the system equations from the element equations. They are chosen to be u_{ij} ($u_{1j} = u_j, u_{2j} = v_j, u_{3j} = w_j$), the x_i ($i = 1,2,3$) components of the translation vectors $\mathbf{u}_j$ at node j ($j = 1,2$), ϕ_{ij}, the x_i ($i = 1,2,3$) components of the rotation vectors $\boldsymbol{\phi}_j$ at node j ($j = 1,2$), and β_j, the twist rate of the shear center axis at node j. Here, the values of $\boldsymbol{\phi}_j$ are reset to zero at the current configuration. Thus, $\delta\phi_{ij}$, the variation of ϕ_{ij}, represents infinitesimal rotations about the x_i axes [32], and the generalized nodal forces corresponding to $\delta\phi_{ij}$ are m_{ij}, the conventional moments about the x_i axes. The generalized nodal forces corresponding to δu_{ij}, the variations of u_{ij}, are f_{ij}, the forces in the x_i directions. The generalized nodal forces corresponding to $\delta\beta_j$, the variations of β_j, are bimoment B_j.

The implicit nodal parameters of the element are used to determine the deformation of the beam element. They are chosen to be u_{ij}, the x_i ($i = 1,2,3$) components of the translation vectors $\mathbf{u}_j$ at node j ($j = 1,2$), θ_{1j}, β_j, v_j', and w_j' ($j = 1,2$) defined in Eq. (17). Let $\theta_{1j}^*, \theta_{2j}^*$ and θ_{3j}^* ($j = 1,2,3$) denote θ_{1j}, $-w_j'$ and v_j', respectively. The generalized nodal forces corresponding to $\delta u_{ij}, \delta\theta_{ij}^*$ and $\delta\beta_j$ are f_{ij}, m_{ij}^θ and B_j, the forces in the x_i directions, the generalized moments, and bimoments, respectively. Note that m_{ij}^θ are not conventional moments, because $\delta\theta_{ij}^*$ are not infinitesimal rotations about the x_i axes at deformed state.

In view of Eqs. (10) and (14), the relations between the variation of the implicit and explicit nodal parameters may be expressed as

$$\delta\mathbf{q}_\theta = \begin{Bmatrix} \delta\mathbf{u}_1 \\ \delta\boldsymbol{\theta}_1^* \\ \delta\mathbf{u}_2 \\ \delta\boldsymbol{\theta}_2^* \\ \delta\boldsymbol{\beta} \end{Bmatrix} = \begin{bmatrix} \mathbf{I}_3 & \mathbf{0} & \mathbf{0} & \mathbf{0} & \bar{\mathbf{0}} \\ \mathbf{T}_{b1} & \mathbf{T}_{a1} & -\mathbf{T}_{b1} & \mathbf{0} & \bar{\mathbf{0}} \\ \mathbf{0} & \mathbf{0} & \mathbf{I}_3 & \mathbf{0} & \bar{\mathbf{0}} \\ \mathbf{T}_{b2} & \mathbf{0} & -\mathbf{T}_{b2} & \mathbf{T}_{a2} & \bar{\mathbf{0}} \\ \bar{\mathbf{0}}^t & \bar{\mathbf{0}}^t & \bar{\mathbf{0}}^t & \bar{\mathbf{0}}^t & \mathbf{I}_2 \end{bmatrix} \begin{Bmatrix} \delta\mathbf{u}_1 \\ \delta\boldsymbol{\phi}_1 \\ \delta\mathbf{u}_2 \\ \delta\boldsymbol{\phi}_2 \\ \delta\boldsymbol{\beta} \end{Bmatrix} = \mathbf{T}_{\theta\phi}\delta\mathbf{q}, \tag{24}$$

$$\mathbf{T}_{bj} = \begin{bmatrix} 0 & 0 & 0 \\ -\theta_{2j}/L & 0 & 0 \\ -\theta_{3j}/L & 0 & 0 \end{bmatrix}, \quad \mathbf{T}_{aj} = \begin{bmatrix} 1 & \theta_{3j}/2 & -\theta_{2j}/2 \\ -\theta_{3j} & 1+\varepsilon_c & 0 \\ \theta_{2j} & 0 & 1+\varepsilon_c \end{bmatrix} \quad (j = 1,2), \tag{25}$$

where $\delta\mathbf{u}_j = \{\delta u_j, \delta v_j, \delta w_j\}$, $\delta\boldsymbol{\theta}_j^* = \{\delta\theta_{1j}, -\delta w_j', \delta v_j'\}$, $\delta\boldsymbol{\phi}_j = \{\delta\phi_{1j}, \delta\phi_{2j}, \delta\phi_{3j}\}$ ($j = 1,2$) and $\delta\boldsymbol{\beta} = \{\delta\beta_1, \delta\beta_2\}$; $\mathbf{I}_2$ and $\mathbf{I}_3$ are the identity matrices of order 2×2 and 3×3, respectively, and $\mathbf{0}$ and $\bar{\mathbf{0}}$ are the zero matrices of order 3×3 and 3×2, respectively.

Let $\mathbf{f} = \{\mathbf{f}_1, \mathbf{m}_1, \mathbf{f}_2, \mathbf{m}_2, \mathbf{B}\}$, $\mathbf{f}_\theta = \{\mathbf{f}_1, \mathbf{m}_1^\theta, \mathbf{f}_2, \mathbf{m}_2^\theta, \mathbf{B}\}$, where $\mathbf{f}_j = \{f_{1j}, f_{2j}, f_{3j}\}$, $\mathbf{m}_j = \{m_{1j}, m_{2j}, m_{3j}\}$, $\mathbf{m}_j^\theta = \{m_{1j}^\theta, m_{2j}^\theta, m_{3j}^\theta\}$ ($j = 1,2$), and $\mathbf{B} = \{B_1, B_2\}$, denote the internal nodal force vectors corresponding to the

variation of the explicit and implicit nodal parameters, $\delta\mathbf{q}$ and $\delta\mathbf{q}_\theta$, respectively. Using the contragradient law [40] and Eq. (24), the relation between $\mathbf{f}$ and $\mathbf{f}_\theta$, may be given by

$$\mathbf{f} = \mathbf{T}^t_{\theta\phi}\mathbf{f}_\theta. \tag{26}$$

The global nodal parameters for the structural system corresponding to the element local nodes j ($j = 1, 2$) should be consistent with the element explicit nodal parameters. Thus, they are chosen to be U_{ij}, the X_i ($i = 1, 2, 3$) components of the translation vectors $\mathbf{U}_j$ at node j ($j = 1, 2$), Φ_{ij}, the X_i ($i = 1, 2, 3$) components of the rotation vectors $\boldsymbol{\Phi}_j$ at nodes j ($j = 1, 2$), and β_j, the twist rate of the shear center axis at node j. Here, the values of $\boldsymbol{\Phi}_j$ are reset to zero at the current configuration. Thus, $\delta\Phi_{ij}$, the variations of Φ_{ij}, represent infinitesimal rotations about the X_i axes [32], and the generalized nodal forces corresponding to $\delta\Phi_{ij}$ are the conventional moments about the X_i axes. The generalized nodal forces corresponding to δU_{ij}, the variation of U_{ij}, are the forces in the X_i directions. The generalized nodal forces corresponding to $\delta\beta_j$, the variation of β_j, are B_j.

2.6. Element nodal force vector

The element nodal force vector $\mathbf{f}_\theta$ (Eq. (26)) corresponding to the implicit nodal parameters is obtained from the virtual work principle in the current element coordinates. It should be mentioned again that the element coordinate system is a local coordinate system not a moving coordinate system. Thus, a standard procedure is used here for the derivation of $\mathbf{f}_\theta$. For convenience, the implicit nodal parameters are divided into four generalized nodal displacement vectors $\mathbf{u}_i$ ($i = a, b, c, d$), where

$$\mathbf{u}_a = \{u_1, u_2\} \tag{27}$$

and $\mathbf{u}_b, \mathbf{u}_c$, and $\mathbf{u}_d$ are defined in Eq. (17).

The generalized force vectors corresponding to $\delta\mathbf{u}_i$, the variation of $\mathbf{u}_i$ ($i = a, b, c, d$), are

$$\begin{aligned}&\mathbf{f}_a = \{f_{11}, f_{12}\}, \quad \mathbf{f}_b = \{f_{21}, m^\theta_{31}, f_{22}, m^\theta_{32}\},\\ &\mathbf{f}_c = \{f_{31}, m^\theta_{21}, f_{32}, m^\theta_{22}\}, \quad \mathbf{f}_d = \{m^\theta_{11}, B_1, m^\theta_{12}, B_2\}.\end{aligned} \tag{28}$$

The virtual work principle requires that

$$\delta\mathbf{u}^t_a\mathbf{f}_a + \delta\mathbf{u}^t_b\mathbf{f}_b + \delta\mathbf{u}^t_c\mathbf{f}_c + \delta\mathbf{u}^t_d\mathbf{f}_d = \int_V (\sigma_{11}\delta\varepsilon_{11} + 2\sigma_{12}\delta\varepsilon_{12} + 2\sigma_{13}\delta\varepsilon_{13})\,\mathrm{d}V, \tag{29}$$

where V is the volume of the undeformed beam, $\delta\varepsilon_{1j}$ ($j = 1, 2, 3$) are the variations of ε_{1j} in Eqs. (21)–(23), respectively, with respect to the implicit nodal parameter. σ_{1j} ($j = 1, 2, 3$) are the second Piola–Kirchhoff stress. For linear elastic material, the following constitutive equations are used:

$$\sigma_{11} = E\varepsilon_{11}, \quad \sigma_{12} = 2G\varepsilon_{12}, \quad \text{and} \quad \sigma_{13} = 2G\varepsilon_{13}, \tag{30}$$

in which E is Young's modulus and G is the shear modulus.

If the element size is chosen to be small enough, the values of the rotation parameters of the deformed element defined in the current element coordinate system may always be much smaller than unity. Thus the higher-order terms of rotation parameters in the element internal nodal forces may be neglected. However, in order to include the nonlinear coupling among the bending, twisting, and stretching deformations, the terms up to the second-order of rotation parameters and their spatial derivatives are retained in element internal nodal forces by consistent second-order linearization of Eq. (29). However the values of $\theta_{1,x}, \theta_{1,xx}, v_{,xx}$, and $w_{,xx}$ in Eqs. (21)–(23) are deformation dependent, not element size dependent. Thus their values may not always be much smaller than unity and their third-order terms may not be negligible. Here, the third-order terms of $\theta_{1,x}, \theta_{1,xx}, v_{,xx}$, and $w_{,xx}$ are also retained in Eq. (29).

From Eqs. (21)–(23), (27)–(30), we may obtain

$$\mathbf{f}_a = \left[AEL\varepsilon_c\left(1+\frac{3}{2}\varepsilon_c\right) + \frac{1}{2}EI_p\int \theta_{1,x}^2\,\mathrm{d}x + \frac{1}{2}EI_y\int w_{,xx}^2\,\mathrm{d}x + \frac{1}{2}EI_z\int v_{,xx}^2\,\mathrm{d}x + \frac{3}{2}EI_\omega\int \theta_{1,xx}^2\,\mathrm{d}x + \underline{EI_{\omega yz}\int \theta_{1,xx}v_{,xx}w_{,xx}\,\mathrm{d}x}\right]\mathbf{G}_a, \tag{31}$$

$$\mathbf{f}_b = EI_z(1+\varepsilon_c)\int \mathbf{N}_b''v_{,xx}\,\mathrm{d}x + f_{12}\mathbf{G}_b + E(I_z-I_y)\int \mathbf{N}_b''\theta_1 w_{,xx}\,\mathrm{d}x + \frac{1}{2}GJ\int(\mathbf{N}_b''\theta_{1,x}w_{,x} - \mathbf{N}_b'\theta_{1,x}w_{,xx})\,\mathrm{d}x + 3EI_{\omega yz}\int \mathbf{N}_b''\theta_{1,xx}w_{,xx}\,\mathrm{d}x + \underline{\frac{3}{2}EK_{\omega z}\int \mathbf{N}_b''\theta_{1,xx}^2v_{,xx}\,\mathrm{d}x + \frac{1}{2}EK_z\int \mathbf{N}_b''v_{,xx}^3\,\mathrm{d}x} + \underline{\frac{3}{2}EK_{yz}\int \mathbf{N}_b''w_{,xx}^2v_{,xx}\,\mathrm{d}x + C_b\int \mathbf{N}_b''\theta_{1,x}^2v_{,xx}\,\mathrm{d}x + \frac{1}{2}EK_{yz}\int \mathbf{N}_b''\theta_{1,x}^2w_{,xx}\,\mathrm{d}x}, \tag{32}$$

$$\mathbf{f}_c = EI_y(1+\varepsilon_c)\int \mathbf{N}_c''w_{,xx}\,\mathrm{d}x + f_{12}\mathbf{G}_c + E(I_z-I_y)\int \mathbf{N}_c''\theta_1 v_{,xx}\,\mathrm{d}x + \frac{1}{2}GJ\int(\mathbf{N}_c'\theta_{1,x}v_{,xx} - \mathbf{N}_c''\theta_{1,x}v_{,x})\,\mathrm{d}x + 3EI_{\omega yz}\int \mathbf{N}_c''\theta_{1,xx}v_{,xx}\,\mathrm{d}x + \underline{\frac{3}{2}EK_{\omega y}\int \mathbf{N}_c''\theta_{1,xx}^2w_{,xx}\,\mathrm{d}x + \frac{1}{2}EK_y\int \mathbf{N}_c''w_{,xx}^3\,\mathrm{d}x} + \underline{\frac{3}{2}EK_{yz}\int \mathbf{N}_c''v_{,xx}^2w_{,xx}\,\mathrm{d}x + C_c\int \mathbf{N}_c''\theta_{1,x}^2w_{,xx}\,\mathrm{d}x + \frac{1}{2}EK_{yz}\int \mathbf{N}_c''\theta_{1,x}^2v_{,xx}\,\mathrm{d}x}, \tag{33}$$

$$\mathbf{f}_d = [GJ+EI_p\varepsilon_c]\int \mathbf{N}_d'\theta_{1,x}\,\mathrm{d}x + EI_\omega(1+3\varepsilon_c)\int \mathbf{N}_d''\theta_{1,xx}\,\mathrm{d}x + E(I_z-I_y)\int \mathbf{N}_d v_{,xx}w_{,xx}\,\mathrm{d}x + \frac{1}{2}GJ\int \mathbf{N}_d'(w_{,x}v_{,xx}-v_{,x}w_{,xx})\,\mathrm{d}x + 3EI_{\omega yz}\int \mathbf{N}_d''v_{,xx}w_{,xx}\,\mathrm{d}x + \underline{\frac{1}{2}EK_I\int \mathbf{N}_d'\theta_{1,x}^3\,\mathrm{d}x} + \underline{\frac{1}{2}EK_\omega\int \mathbf{N}_d''\theta_{1,xx}^3\mathrm{d}x + 2EI_{\omega yz}\int \mathbf{N}_d\theta_{1,xx}(w_{,xx}^2-v_{,xx}^2)\,\mathrm{d}x + C_b\int \mathbf{N}_d'v_{,xx}^2\theta_{1,x}\,\mathrm{d}x + C_c\int \mathbf{N}_d'w_{,xx}^2\theta_{1,x}\,\mathrm{d}x} + \underline{\frac{3}{2}EK_{\omega z}\int \mathbf{N}_d''v_{,xx}^2\theta_{1,xx}\,\mathrm{d}x + \frac{3}{2}EK_{\omega y}\int \mathbf{N}_d''w_{,xx}^2\theta_{1,xx}\,\mathrm{d}x + C_d\int(\mathbf{N}_d'\theta_{1,xx}^2\theta_{1,x} + \mathbf{N}_d''\theta_{1,x}^2\theta_{1,xx})\,\mathrm{d}x}, \tag{34}$$

where

$$\mathbf{G}_a = \frac{1}{L}\{-1,1\},\quad \mathbf{G}_b = \int \mathbf{N}_b'v_{,x}\,\mathrm{d}x,\quad \mathbf{G}_c = \int \mathbf{N}_c'w_{,x}\,\mathrm{d}x, \tag{35}$$

$$I_y = \int z^2\,\mathrm{d}A,\quad I_z = \int y^2\,\mathrm{d}A,\quad I_p = I_y + I_z,\quad I_{\omega yz} = \int \omega yz\,\mathrm{d}A,\quad I_\omega = \int \omega^2\,\mathrm{d}A,$$

$$C_b = \frac{1}{2}E(K_z + K_{yz} + 4I_{\omega yz}) + GJ_z,\quad C_c = \frac{1}{2}E(K_y + K_{yz} - 4I_{\omega yz}) + GJ_y,$$

$$C_d = \frac{1}{2}E(K_{\omega y} + K_{\omega z}) + GJ_\omega,\quad K_y = \int z^4\,\mathrm{d}A,\quad K_{yz} = \int y^2z^2\mathrm{d}A,\quad K_z = \int y^4\,\mathrm{d}A,$$

$$K_1 = K_y + K_z + 2K_{yz},\quad K_\omega = \int \omega^4\,\mathrm{d}A,\quad K_{\omega y} = \int \omega^2z^2\,\mathrm{d}A,\quad K_{\omega z} = \int \omega^2y^2\,\mathrm{d}A,$$

$$J = \int\left[(-z+\omega_{,y})^2 + (y+\omega_{,z})^2\right]\mathrm{d}A,\quad J_y = \int\left[(z\omega_{,z}-\omega)^2 + z^2\omega_{,y}^2\right]\mathrm{d}A,$$

$$J_z = \int \left[(\omega - y\omega_{,y})^2 + y^2\omega_{,z}^2\right] \mathrm{d}A, \quad J_\omega = \int \omega^2 \left(\omega_{,y}^2 + \omega_{,z}^2\right) \mathrm{d}A \tag{36}$$

in which the range of integrations for the integral $\int(\,)\,\mathrm{d}x$ in Eqs. (31)–(36) is from 0 to L, A is the cross-sectional area, and $\mathbf{N}_j$ ($j = b, c, d$) are given in Eq. (18). The underlined terms in Eqs. (31)–(34) are the third-order terms of $\theta_{1,x}, \theta_{1,xx}, v_{,xx}$, and $w_{,xx}$.

The element nodal force vector $\mathbf{f}$ (Eq. (26)) corresponding to the explicit nodal parameters may be obtained from Eqs. (26) and (31)–(34). Note that only the terms up to the second-order of nodal parameters and the third-order terms of $\theta_{1,x}, \theta_{1,xx}, v_{,xx}$, and $w_{,xx}$ are retained in $\mathbf{f}_\theta$. Thus, the corresponding $\mathbf{f}$ in Eq. (26) may be rewritten as

$$\mathbf{f} = \mathbf{f}_\theta + \left(\mathbf{T}_{\theta\phi}^t - \mathbf{I}_{14}\right)\mathbf{f}_\theta^1, \tag{37}$$

where $\mathbf{f}_\theta^1$ are the first-order terms of nodal parameters of $\mathbf{f}_\theta$, and $\mathbf{I}_{14}$ is the identity matrix of order 14×14.

2.7. Element tangent stiffness matrices

The element tangent stiffness matrix corresponding to the explicit nodal parameters (referred to as explicit tangent stiffness matrix) may be obtained by differentiating the element nodal force vector $\mathbf{f}$ in Eq. (37) with respect to explicit nodal parameters. Using Eqs. (24) and (37), we obtain

$$\mathbf{k} = \frac{\partial \mathbf{f}}{\partial \mathbf{q}} = \frac{\partial \mathbf{f}}{\partial \mathbf{q}_\theta}\frac{\partial \mathbf{q}_\theta}{\partial \mathbf{q}} = \left[\mathbf{k}_\theta + \left(\mathbf{T}_{\theta\phi}^t - \mathbf{I}_{14}\right)\mathbf{k}_\theta^0 + \mathbf{H}\right]\mathbf{T}_{\theta\phi}, \tag{38}$$

where $\mathbf{k}_\theta = \partial \mathbf{f}_\theta / \partial \mathbf{q}_\theta$ is the tangent stiffness matrix corresponding to implicit nodal parameters (referred to as implicit tangent stiffness matrix), $\mathbf{k}_\theta^0$ are the zeroth-order terms of nodal parameters of $\mathbf{k}_\theta$, and $\mathbf{H}$ is a unsymmetrical matrix and is given by

$$\mathbf{H} = \begin{bmatrix} \mathbf{0} & \mathbf{h}_{b1} & \mathbf{0} & \mathbf{h}_{b2} & \bar{\mathbf{0}} \\ \mathbf{h}_{b1}^t & \mathbf{h}_{a1} & -\mathbf{h}_{b1}^t & \mathbf{0} & \bar{\mathbf{0}} \\ \mathbf{0} & -\mathbf{h}_{b1} & \mathbf{0} & -\mathbf{h}_{b2} & \bar{\mathbf{0}} \\ \mathbf{h}_{b2}^t & \mathbf{0} & -\mathbf{h}_{b2}^t & \mathbf{h}_{a2} & \bar{\mathbf{0}} \\ \bar{\mathbf{0}}^t & \bar{\mathbf{0}}^t & \bar{\mathbf{0}}^t & \bar{\mathbf{0}}^t & \mathbf{0}_2 \end{bmatrix}, \tag{39}$$

$$\mathbf{h}_{bj} = \begin{bmatrix} 0 & -(1/L)m_{2j}^\theta & -(1/L)m_{3j}^\theta \\ 0 & 0 & 0 \\ 0 & 0 & 0 \end{bmatrix}, \quad \mathbf{h}_{aj} = \begin{bmatrix} 0 & m_{3j}^\theta & -m_{2j}^\theta \\ 0 & 0 & (1/2)m_{1j}^\theta \\ 0 & -(1/2)m_{1j}^\theta & 0 \end{bmatrix} \quad (j = 1, 2, 3), \tag{40}$$

where $\mathbf{0}_2, \mathbf{0}$ and $\bar{\mathbf{0}}$ are the zero matrices of order 2×2, 3×3 and 3×2, respectively.

Using the direct stiffness method, the implicit tangent stiffness matrix $\mathbf{k}_\theta$ may be assembled by the submatrices

$$\mathbf{k}_{ij} = \frac{\partial \mathbf{f}_i}{\partial \mathbf{u}_j}, \tag{41}$$

where $\mathbf{f}_i$ ($i = a, b, c, d$) are defined in Eqs. (31)–(34) and $\mathbf{u}_i$ ($i = a, b, c, d$) are defined in Eqs. (17) and (27). Note that $\mathbf{k}_{ij}$ are the symmetric matrices. The explicit form of $\mathbf{k}_{ij}$ may be expressed as

$$\mathbf{k}_{aa} = AEL(1 + 3\varepsilon_c)\mathbf{G}_a\mathbf{G}_a^t,$$

$$\mathbf{k}_{ab} = \mathbf{G}_a\left(AE\mathbf{G}_b^t + EI_z\int \mathbf{N}_b'^t v_{,xx}\,\mathrm{d}x + \underline{EI_{\omega yz}\int \mathbf{N}_b''^t \theta_{1,xx}w_{,xx}\,\mathrm{d}x}\right),$$

$$\mathbf{k}_{ac} = \mathbf{G}_a\left(AE\mathbf{G}_c^t + EI_y\int \mathbf{N}_b''^t w_{,xx}\,dx + \underline{EI_{\omega yz}\int \mathbf{N}_b''^t\theta_{1,xx}v_{,xx}\,dx}\right),$$

$$\mathbf{k}_{ad} = \mathbf{G}_a\left(EI_p\int \mathbf{N}_d'^t\theta_{1,x}\,dx + 3EI_\omega\int \mathbf{N}_d''^t\theta_{1,xx}\,dx + \underline{EI_{\omega yz}\int \mathbf{N}_d''^t v_{,xx}w_{,xx}\,dx}\right),$$

$$\mathbf{k}_{bb} = EI_z(1+\varepsilon_c)\int \mathbf{N}_b''\mathbf{N}_b''^t\,dx + f_{12}\int \mathbf{N}_b'\mathbf{N}_b'^t\,dx + \underline{\frac{3}{2}EK_{\omega z}\int \mathbf{N}_b''\mathbf{N}_b''^t\theta_{1,xx}^2\,dx + \frac{3}{2}EK_z\int \mathbf{N}_b''\mathbf{N}_b''^t v_{,xx}^2\,dx + \frac{3}{2}EK_{yz}\int \mathbf{N}_b''\mathbf{N}_b''^t w_{,xx}^2\,dx + C_b\int \mathbf{N}_b''\mathbf{N}_b''^t\theta_{1,x}^2\,dx},$$

$$\mathbf{k}_{bc} = E(I_z-I_y)\int \mathbf{N}_b''\mathbf{N}_c''^t\theta_1\,dx + 3EI_{\omega yz}\int \mathbf{N}_b''\mathbf{N}_c''^t\theta_{1,xx}\,dx + \frac{1}{2}GJ\int(\mathbf{N}_b''\mathbf{N}_c'^t - \mathbf{N}_b'\mathbf{N}_c''^t)\theta_{1,x}\,dx + \underline{EK_{yz}\int \mathbf{N}_b''\mathbf{N}_c''^t\left(3v_{,xx}w_{,xx} + \frac{1}{2}\theta_{1,x}^2\right)dx},$$

$$\mathbf{k}_{bd} = E(I_z-I_y)\int \mathbf{N}_b''\mathbf{N}_d^t w_{,xx}\,dx + \frac{1}{2}GJ\int(\mathbf{N}_b''\mathbf{N}_d'^t w_{,x} - \mathbf{N}_b'\mathbf{N}_d'^t w_{,xx})\,dx + 3EI_{\omega yz} \times \int \mathbf{N}_b''\mathbf{N}_d''^t w_{,xx}\,dx + \underline{3EK_{\omega z}\int \mathbf{N}_b''\mathbf{N}_b''^t\theta_{1,xx}v_{,xx}\,dx} + \underline{2C_b\int \mathbf{N}_b''\mathbf{N}_d'^t\theta_{1,x}v_{,xx}\,dx + EK_{yz}\int \mathbf{N}_b''\mathbf{N}_d'^t\theta_{1,x}w_{,xx}\,dx},$$

$$\mathbf{k}_{cc} = EI_y(1+\varepsilon_c)\int \mathbf{N}_c''\mathbf{N}_c''^t\,dx + f_{12}\int \mathbf{N}_c'\mathbf{N}_c'^t\,dx + \underline{\frac{3}{2}EK_{\omega y}\int \mathbf{N}_c''\mathbf{N}_c''^t\theta_{1,xx}^2\,dx + \frac{3}{2}EK_y\int \mathbf{N}_c''\mathbf{N}_c''^t w_{,xx}^2\,dx + \frac{3}{2}EK_{yz}\int \mathbf{N}_c''\mathbf{N}_c''^t v_{,xx}^2\,dx + C_c\int \mathbf{N}_c''\mathbf{N}_c''^t\theta_{1,x}^2\,dx},$$

$$\mathbf{k}_{cd} = E(I_z-I_y)\int \mathbf{N}_c''\mathbf{N}_d^t v_{,xx}\,dx + \frac{1}{2}GJ\int(\mathbf{N}_c'\mathbf{N}_d'^t v_{,xx} - \mathbf{N}_c''\mathbf{N}_d't v_{,x})\,dx + 3EI_{\omega yz} \times \int \mathbf{N}_c''\mathbf{N}_d''^t v_{,xx}\,dx + \underline{3EK_{\omega y}\int \mathbf{N}_c''\mathbf{N}_d''^t\theta_{1,xx}w_{,xx}\,dx + 2C_c\int \mathbf{N}_c''\mathbf{N}_d'^t\theta_{1,x}w_{,xx}\,dx + EK_{yz}\int \mathbf{N}_c''\mathbf{N}_d'^t\theta_{1,x}v_{,xx}\,dx},$$

$$\mathbf{k}_{dd} = [GJ + EI_p\varepsilon_c]\int \mathbf{N}_d'\mathbf{N}_d'^t\,dx + EI_\omega(1+3\varepsilon_c)\int \mathbf{N}_d''\mathbf{N}_d''^t\,dx + \underline{\frac{3}{2}EK_I\int \mathbf{N}_d'\mathbf{N}_d'^t\theta_{1,x}^2\,dx} + \underline{\frac{3}{2}EK_\omega\int \mathbf{N}_d''\mathbf{N}_d''^t\theta_{1,xx}^2\,dx + 2EI_{\omega yz}\int \mathbf{N}_d\mathbf{N}_d''^t(w_{,xx}^2 - v_{,xx}^2)\,dx} + \underline{C_b\int \mathbf{N}_d'\mathbf{N}_d'^t v_{,xx}^2\,dx + C_c\int \mathbf{N}_d'\mathbf{N}_d'^t tw_{,xx}^2\,dx + \frac{3}{2}EK_{\omega z}\int \mathbf{N}_d''\mathbf{N}_d''^t v_{,xx}^2\,dx} + \underline{\frac{3}{2}EK_{\omega y}\int \mathbf{N}_d''\mathbf{N}_d''t w_{,xx}^2 dx + C_d\int\left[\mathbf{N}_d'\mathbf{N}_d'^t\theta_{1,xx}^2 + \mathbf{N}_d''\mathbf{N}_d''t\theta_{1,x}^2 + 2(\mathbf{N}_d'\mathbf{N}_d''^t + \mathbf{N}_d''\mathbf{N}_d'^t)\theta_{1,x}\theta_{1,xx}\right]dx}, \quad (42)$$

where the underlined terms are the second-order terms of $\theta_{1,x}, \theta_{1,xx}, v_{,xx}$, and $w_{,xx}$.

The element tangent stiffness matrix referred to the global coordinate system is obtained by using the standard coordinate transformation.

2.8. Load stiffness matrix

Different ways for generating configuration-dependent moment were proposed in the literature [8,10,33,41]. Here, for simplicity, only the conservative moments generated by conservative force or

forces (with fixed directions) are considered, and the ways for generating conservative moment proposed in [33] are employed here. For completeness, a brief description of the ways for generating conservative moment is given here. In this study, a set of load base coordinates X_i^P $(i = 1, 2, 3)$ associated with each configuration-dependent moment is constructed at the current configuration. The mechanism for generating configuration-dependent moment is described in these coordinates, and the corresponding external load and load stiffness matrix [42] are defined in terms of these coordinates. Unless stated otherwise, all vectors and matrices in this section are referred to these coordinates. Note that this coordinate system is just a local coordinate system constructed at the current configuration, not a moving coordinate system. Thus, it is regarded as a fixed coordinated system in the derivation of the load stiffness matrix.

The first way for generating configuration-dependent moment may described as follows.

Consider a sphere of radius R whose centroid is rigidly connected with the structure at node O as shown in Fig. 3. Two strings wound around a great circle of the sphere are acted upon by forces of magnitude P. Thus, the strings are always tangent to the sphere. The great circle and the forces are on the same plane at the undeformed configuration of the structure. However, the great circle and the forces are generally not on the same plane when the structure is deformed. The origin of the load base coordinate system is chosen to be located at the node O. The X_1^P axis is chosen to coincide with the normal of the plane of the great circle, and the X_2^P and X_3^P axes lie in the plane of the great circle.

Let A denote the contact point of the force $\mathbf{P}$ and the great circle. Because $\mathbf{P}$ is tangent to the sphere, $\mathbf{P}$ is perpendicular to the line OA. Let $\mathbf{e}_A$ denote the unit vector in the direction of line OA. $\mathbf{e}_A$ may be expressed by

$$\mathbf{e}_A = \mathbf{a}/(\mathbf{a}^t\mathbf{a})^{1/2}, \tag{43}$$

$$\mathbf{a} = \mathbf{e}_p^P \times \mathbf{n}^P = \{0, \ell_3, -\ell_2\}, \tag{44}$$

where $\mathbf{e}_p^P = \{\ell_1, \ell_2, \ell_3\}$ is the unit vector in the direction of $\mathbf{P}$, and $\mathbf{n}^P$ is the unit normal of the plane of the great circle. Note that $\mathbf{n}^P$ coincides with $\mathbf{e}_1^P = \{1, 0, 0\}$, the unit vector associated with the X_1^P axis.

The external moment vector at node O generated by the above-mentioned mechanism may be expressed by

$$\mathbf{M} = M\,\mathbf{e}_A \times \mathbf{e}_p^P, \tag{45}$$

where $M = 2RP$ is the magnitude of the moment. The corresponding load stiffness matrix $\mathbf{k}_p$ may be expressed as

$$\mathbf{k}_p = M(\ell_2^2 + \ell_3^2)^{-1/2}\mathbf{k}_{pa} + M(\ell_2^2 + \ell_3^2)^{-3/2}\mathbf{k}_{pb}, \tag{46}$$

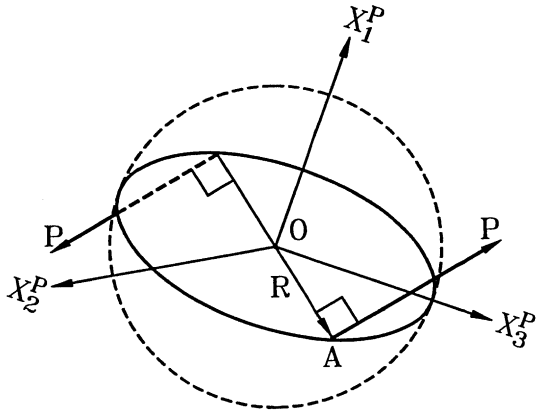

Fig. 3. Mechanism for generating configuration-dependent moment.

where

$$\mathbf{k}_{pa} = \begin{bmatrix} 0 & \ell_1\ell_3 & -\ell_1\ell_2 \\ 0 & \ell_2\ell_3 & \ell_1^2+\ell_3^2 \\ 0 & -\ell_1^2-\ell_2^2 & -\ell_2\ell_3 \end{bmatrix}, \tag{47}$$

$$\mathbf{k}_{pb} = \begin{bmatrix} 0 & -\ell_1\ell_3(\ell_2^2+\ell_3^2) & \ell_1\ell_2(\ell_2^2+\ell_3^2) \\ 0 & \ell_1^2\ell_2\ell_3 & -\ell_1^2\ell_2^2 \\ 0 & \ell_1^2\ell_3^2 & -\ell_1^2\ell_2\ell_3 \end{bmatrix}. \tag{48}$$

Three special cases shown in Fig. 4 are considered here. Following [10], they are referred to as quasitangential (QT) moments of the first and second types, and semitangential (ST) moment. The load stiffness matrices corresponding to QT and ST moment at the configurations shown in Fig. 4 may be obtained from Eqs. (46)–(48) and given by

$$\mathbf{k}_p^{\mathrm{QT1}} = M \begin{bmatrix} 0 & 0 & 0 \\ 0 & 0 & 0 \\ 0 & -1 & 0 \end{bmatrix}, \tag{49}$$

$$\mathbf{k}_p^{\mathrm{QT2}} = M \begin{bmatrix} 0 & 0 & 0 \\ 0 & 0 & 1 \\ 0 & 0 & 0 \end{bmatrix}, \tag{50}$$

$$\mathbf{k}_p^{\mathrm{ST}} = \frac{M}{2} \begin{bmatrix} 0 & 0 & 0 \\ 0 & 0 & 1 \\ 0 & -1 & 0 \end{bmatrix}. \tag{51}$$

The second way for generating configuration-dependent moment may described as follows.

Consider a rigid arm of length R which end is rigidly connected with the structure at node O as shown in Fig. 5. The other end of the rigid arm is acted upon by a conservative force (with a fixed direction) of magnitude P. The origin of the load base coordinates X_i^P $(i = 1, 2, 3)$ is chosen to be located at the node O. The X_1^P axis is chosen to coincide with the axis of the rigid arm, and the X_2^P and X_3^P axes are perpendicular to the rigid arm.

The external moment vector at node O generated by the above-mentioned mechanism may be expressed by

$$\mathbf{M} = RP\mathbf{t}^P \times \mathbf{e}_p^P, \tag{52}$$

where $\mathbf{e}_p^P = \{\ell_1, \ell_2, \ell_3\}$ is the unit vector in the direction of $\mathbf{P}$, and $\mathbf{t}^P$ is the unit vector in the axial direction of the rigid arm. Note that $\mathbf{t}^P$ coincides with $\mathbf{e}_1^P = \{1, 0, 0\}$, the unit vector associated with the X_1^P axis. The corresponding load stiffness matrix may be expressed as

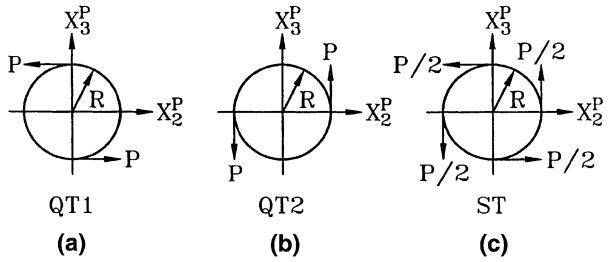

Fig. 4. Quasitangential (QT) moment and semitangential (ST) moment.

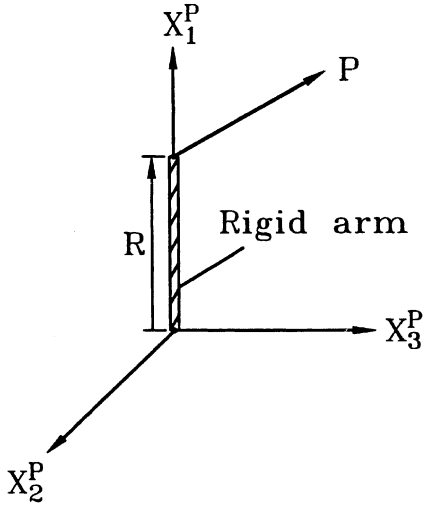

Fig. 5. Mechanism for generating configuration-dependent moment by an off-axis load.

$$\mathbf{k}_p = RP \begin{bmatrix} 0 & \ell_2 & \ell_3 \\ 0 & -\ell_1 & 0 \\ 0 & 0 & -\ell_1 \end{bmatrix}. \tag{53}$$

The load stiffness matrix referred to the global coordinate system is obtained by using the standard coordinate transformation and may be expressed by

$$\mathbf{k}_p^G = \mathbf{A}_{GP}\mathbf{k}_p\mathbf{A}_{GP}^t, \tag{54}$$

where $\mathbf{A}_{GP}$ is the transformation matrix given in Eq. (1).

2.9. Equilibrium equations

The nonlinear equilibrium equations may be expressed by

$$\Psi = \mathbf{F} - \lambda\mathbf{P} = \mathbf{0}, \tag{55}$$

where Ψ is the unbalanced force between the internal nodal force $\mathbf{F}$ and the external nodal force $\lambda\mathbf{P}$, where λ is the loading parameter, and $\mathbf{P}$ is a reference loading. Note that $\mathbf{P}$ may require to be updated at each iteration if the applied load is configuration dependent. $\mathbf{F}$ is assembled from the element nodal force vectors, which are calculated using Eqs. (31)–(34) and (37) first in the current element coordinates and then transformed from current element coordinate system to global coordinate system before assemblage using standard procedure.

In this paper, a weighted Euclidean norm of the unbalanced force is employed as the error measure for the equilibrium iterations, and is given by

$$\frac{\|\Psi\|}{|\lambda|\sqrt{N}} \leqslant e_{\text{tol}}, \tag{56}$$

where N is the number of equilibrium equations; e_{tol} is a prescribed value of error tolerance.

2.10. Criterion of the buckling state

Here, the zero value of the tangent stiffness matrix determinant is used as the criterion of the buckling state. The tangent stiffness matrix of the structure is assembled from the element stiffness matrix and load

stiffness matrix. Let $\mathbf{K}_T(\lambda)$ denote the tangent stiffness matrix of the structure corresponding to the loading parameter λ. The criterion of the buckling state may be expressed as

$$D(\lambda) = \det|\mathbf{K}_T(\lambda)| = 0. \tag{57}$$

Let λ_{NB} denote the minimum loading parameter satisfying Eq. (57). λ_{NB} is called the buckling loading parameter here.

The buckling mode corresponding to λ_{NB} may be obtained by solving the following generalized eigenvalue problem

$$\mathbf{K}_0\mathbf{X} = -\frac{\lambda}{\lambda_{NB}}\mathbf{K}_G\mathbf{X}, \tag{58}$$

where $\mathbf{K}_0$ is the linear stiffness matrix of the structure, and $\mathbf{K}_G = \mathbf{K}_T - \mathbf{K}_0$ is the geometric stiffness matrix of the structure corresponding to λ_{NB}. It can be seen that λ_{NB} is also an eigenvalue for Eq. (58). The eigenvector corresponding to eigenvalue λ_{NB} is the required buckling mode. Here, the inverse power method [43] is used to find the buckling mode.

3. Numerical algorithm

An incremental-iterative method based on the Newton–Raphson method combined with constant arc length of incremental displacement vector [44,45] is employed for the solution of nonlinear equilibrium equations. For a given displacement increment or corrector, the method described in [32,46] is employed to determine the current element cross-section coordinates, element coordinates and element deformation nodal parameters for each element. A parabolic interpolation method of the arc length is employed here to find the buckling load. In order to initiate the secondary path, at the bifurcation point a perturbation displacement proportional to the first buckling mode is added [47].

The basic steps involved in the parabolic interpolation method are outlined as follows.

Assume that the equilibrium configuration of the Ith incremental step is obtained. Let ΔS_I denote the arc length of the incremental displacement vector of the Ith incremental step, λ_I and $\mathbf{K}_T^I$ denote the loading parameter and tangent stiffness matrix corresponding to the equilibrium configuration of the Ith incremental step, respectively, and $D(\lambda_I)$ denotedet $|\mathbf{K}_T^I|$. If $\mathbf{K}_T^{I-1}$ is positive definite and $\mathbf{K}_T^I$ is positive nondefinite, the following steps are used to obtain the buckling load.

1. Let $\Delta S_L = 0$, $\Delta S_R = \Delta S_I$, $\lambda_L = 0$, $\lambda_R = \lambda_I$, $D_L = D(\lambda_{I-1})$, and $D_R = D(\lambda_I)$.
2. Let $\Delta S_I = \frac{1}{2}(\Delta S_L + \Delta S_R)$.
3. Repeat the Ith incremental step to obtain a new λ_I, $\mathbf{K}_T^I$ and $D(\lambda_I)$.
4. If $\mathbf{K}_T^I$ is positive definite, let $\lambda_M = \lambda_L$, $\Delta S_M = \Delta S_L$, $D_M = D_L$, $\lambda_L = \lambda_I$, $\Delta S_L = \Delta S_I$, and $D_L = D(\lambda_I)$. If $\mathbf{K}_T^I$ is positive nondefinite, let $\lambda_M = \lambda_R$, $\Delta S_M = \Delta S_R$, $D_M = D_R$, $\lambda_R = \lambda_I$, $\Delta S_R = \Delta S_I$, and $D_R = D(\lambda_I)$.
5. Let $\lambda_I = (\lambda_L + \lambda_R)/2$. If $|\lambda_L - \lambda_R|/\lambda_I \leqslant E_\lambda$, where E_λ is a prescribed error tolerance, stop the iteration; otherwise go to step 6.
6. Let $\bar{D}(\Delta S) = a\Delta S^2 + b\Delta S + c$ denote the parabola that passes through points $(\Delta S_L,\ D_L)$, $(\Delta S_M,\ D_M)$ and $(\Delta S_R,\ D_R)$. If $b^2 - 4ac \geqslant 0$, let ΔS_1 and ΔS_2 be the solutions of $\bar{D}(\Delta S) = 0$. If $\Delta S_L < \Delta S_i < \Delta S_R$ $(i = 1, 2)$, let $\Delta S_I = \frac{1}{2}(\Delta S_1 + \Delta S_2)$. If $\Delta S_L < \Delta S_i < \Delta S_R$ $(i = 1$ or $2)$, let $\Delta S_I = \Delta S_i$. If $\Delta S_R \leqslant \Delta S_i$ or $\Delta S_L \geqslant \Delta S_i$ $(i = 1, 2)$, let $\Delta S_I = \frac{1}{2}(\Delta S_L + \Delta S_R)$. If $b^2 - 4ac < 0$, let $\Delta S_I = \frac{1}{2}(\Delta S_L + \Delta S_R)$.
7. Go to step 3.

The buckling load λ_{NB} is chosen to be the converged λ_I.

4. Numerical studies

In order to investigate the effect of the third-order terms of the element nodal forces on the buckling load and post-buckling behavior of three-dimensional beams, the following cases are considered:

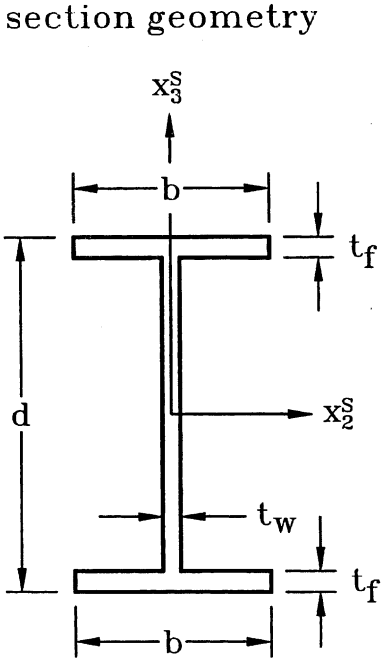

Fig. 6. Geometry of I section.

1. NF = 1: All the terms up to the second-order in Eqs. (31)–(34) and the third-order term of the twist rate, $\frac{1}{2}EK_I \int \mathbf{N}'_d \theta^3_{1,s}\,ds$ in Eq. (34), and the corresponding terms in Eq. (42) are considered.
2. NF = 2: All the terms in Eqs. (31)–(34), and Eq. (42) are considered.

Here only the beams with rectangular cross-section and doubly symmetrical I sections shown in Fig. 6 are considered. The approximated Saint Venant warping function of the thin-walled I section used here is given by

$$\omega = \begin{cases} -y(z-d+t_f) & \text{for top flange} \quad (-0.5b \leqslant y \leqslant 0.5b,\ 0.5d - t_f \leqslant z \leqslant 0.5d), \\ yz & \text{for web} \quad (-0.5b \leqslant y \leqslant 0.5b,\ 0.5d - t_f \leqslant z \leqslant 0.5d), \\ -y(z+d-t_f) & \text{for bottom flange} \quad (-0.5b \leqslant y \leqslant 0.5b,\ -0.5d \leqslant z \leqslant 0.5d - t_f). \end{cases}$$

For convenience, in this study, WF and WR are used to denote that the cross-sections are warping free and warping restrained, respectively.

Example 1 (*Cantilever beam subjected to end torque*). The example considered here is a W21× 93 cantilever beam subjected to an end torque T as shown in Fig. 7. Three different warping boundary conditions are considered: (a) WF at both ends of the beam; (b) WR at fixed end of the beam and WF at free end of the beam; (c) WR at both ends of the beam. Since only the primary path is considered for this example, the ways of generating end moment are rendered irrelevant here. The geometry and material properties are: $L = 240$ in.; $b = 8.42$ in.; $t_f = 0.93$ in.; $d = 21.62$ in.; $t_w = 0.58$ in.; Young's modulus $E = 29{,}000$ ksi, and the shear modulus $G = 11{,}200$ ksi. It is noted that the only nonzero deformations are $\theta_{1,x}, \theta_{1,xx}$ and ε_c for this example. The present results are obtained by using 20 elements and shown in Fig. 8. The results of NF = 1 and 2 are nearly identical for this example. Thus only the results of NF = 1 are shown in Fig. 8. As can be seen the torsional stiffness increases with the increase of the twist angle. It indicates that the effect of the third-order term of the twist rate is not negligible when the twist angle is not small for this example.

Example 2 (*Cantilever beam subjected to end force* (*buckling analysis*)). The buckling load of the I-section cantilever beam subjected to a vertical end force P as shown in Fig. 9 is studied here. This example was investigated experimentally and theoretically by Anderson and Trahair [5] and also studied by Pi and

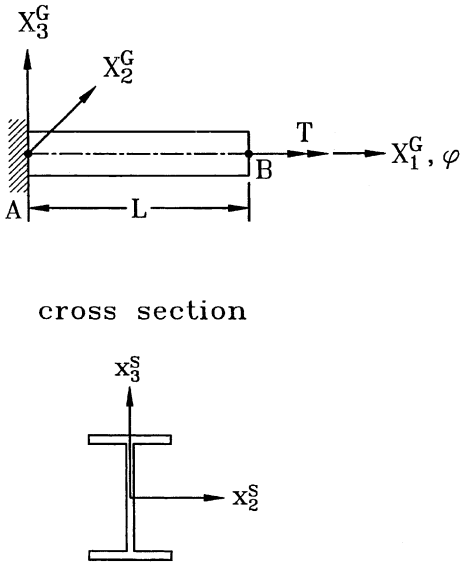

Fig. 7. Cantilever beam subjected to end torque.

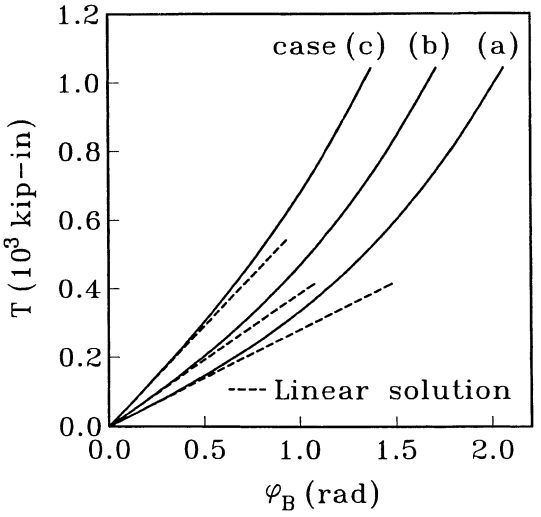

Fig. 8. Load-end twist angle for cantilever beam subjected to end torque.

Trahair [24] using the finite element method. The clamped end of the beam is fully restrained against warping, and the free end is warping free. The geometry and material properties of the beam are: $b = 1.241$ in.; $t_f = 0.1232$ in.; $h = 2.975$ in.; $t_w = 0.0862$ in.; Young's modulus $E = 9,444,854$ psi, and the shear modulus $G = 3,766,629$ psi. The present results for NF = 1 and 2 obtained by using 5 and 10 elements are all nearly identical. The present buckling loads for NF = 1 obtained by using five elements are shown in Table 1 together with those given in [5,24]. It can be seen that the agreement among these solutions given in Table 1 is very good.

Example 3 (*Cantilever beam subjected to end force* (*post-buckling analysis*)). The example considered here is an I-shaped cantilever beam with a vertical force P applied at the centroid of the end cross-section as shown in Fig. 10. The clamped end of the beam is fully restrained against warping, and the free end is warping free.

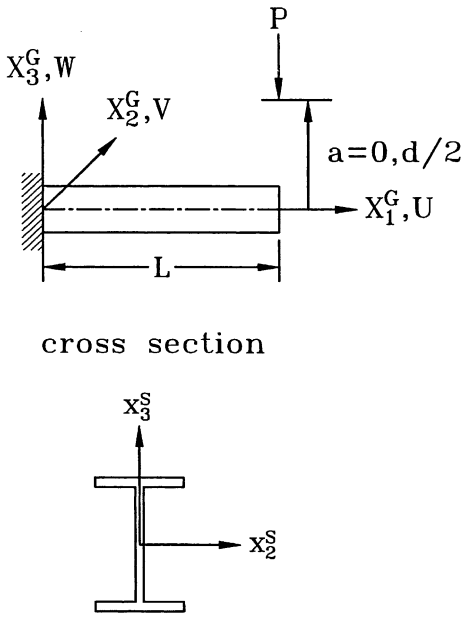

Fig. 9. Cantilever beam subjected to end force (buckling analysis).

Table 1
Buckling load for cantilever beam subjected to end force

Load applied at	L (in.)	Buckling load P_{NB} (lb)			
		Exp. [5]	Theory [5]	FEM [24]	Present
Upper face	50	91.2	94.6	92.1	91.8
	65	59.7	56.8	56.5	56.2
Centroid	50	134.2	139.2	141.8	138.1
	65	72.7	74.2	76.1	74.5

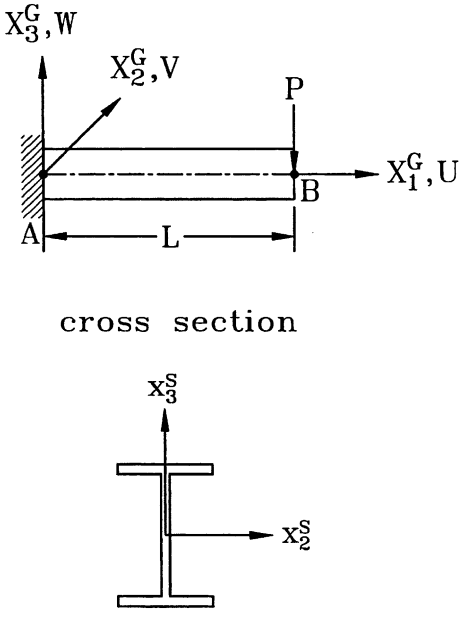

Fig. 10. Cantilever beam subjected to end force (post-buckling analysis).

Here, three cases studied in the literature are considered. The geometrical and material properties are: (1) $L = 10$ m, $b = 0.19$ m, $t_f = 0.013$ m, $d = 0.613$ m, $t_w = 0.025$ m, Young's modulus $E = 206 \times 10^9$ N/m^2, and Poisson's ratio $v = 0.3$ [29]; (2) $L = 130$ in., $b = 0.86$ in., $t_f = 0.122$ in., $d = 2.984$ in., $t_w = 0.085$ in., Young's modulus $E = 9,300,000$ psi, the shear modulus $G = 3,698,534$ psi and the self-weight is 0.0436 lb/in. [6] and (3) $L = 4800$ mm, $b = 300$ mm, $t_f = 25$ mm $d = 325$ mm, $t_w = 25$ mm, Young's modulus $E = 200,000$ N/mm^2, and Poisson's ratio $v = 0.3$ [48]. The present results are obtained using 40 elements for cases (1), (2) and 80 elements for case (3). The results for NF = 1 and 2 are nearly identical for this example. Thus only the results for NF = 1 are given here. The present buckling loads are $P_{NB} = 47.333$ kN for case (1), $P_{NB} = 5.751$ lb for case (2), and $P_{NB} = 1015.661$ kN for case (3). The linear buckling loads [2] are 46.359 lb and 833.32 kN for cases (1) and (3), respectively. The ratios of the minor axis (out-of-plane) flexural stiffness to the major axis (in-plane) flexural stiffness are 0.018 and 0.296 for cases (1) and (3), respectively. Because this ratio is large for case (3), the difference between the nonlinear buckling load and linear buckling load is significant for case (3). The load–deflection curves of the present study together with the results given in the literature are shown in Figs. 11–13. In Fig. 11, the results of [29] are obtained by

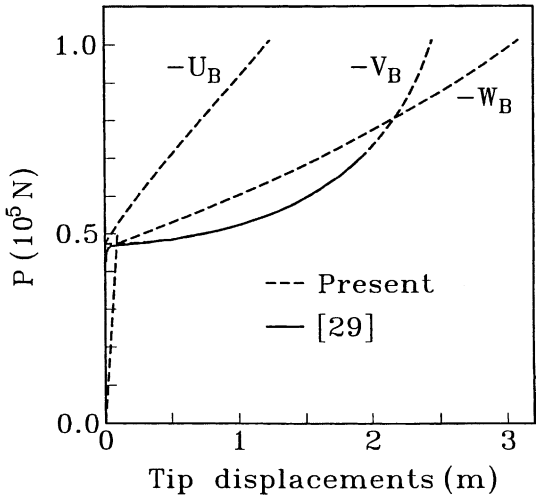

Fig. 11. Load–tip displacements for cantilever beam subjected to end force (case 1).

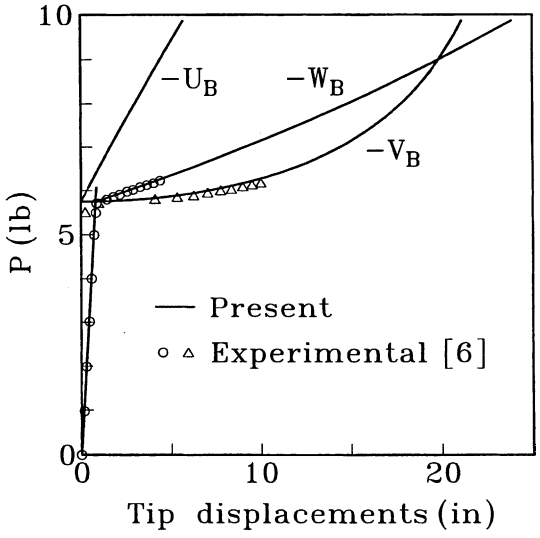

Fig. 12. Load–tip displacements for cantilever beam subjected to end force (case 2).

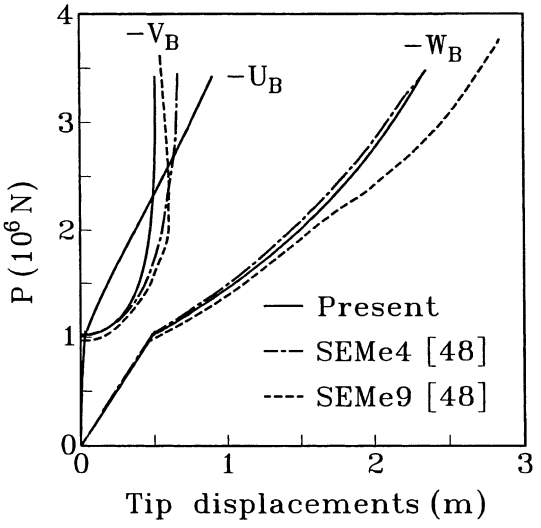

Fig. 13. Load–tip displacements for cantilever beam subjected to end force (case 3).

considering a small twist imperfection, which varies linearly from zero value at the support to a value of 10^{-3} radian at the tip. In Fig. 12, the initial deflections caused by the self-weight are excluded. In Fig. 13, the results of [48] are obtained by 48 4-node and 9-node stress resultant based semimixed shell elements, SEMe4 and SEMe9, respectively. It can beseen that the agreement among these solutions given in Figs. 11–13 is quite good.

Example 4 (*Simply supported beam subjected to eccentric axial force*). This example was first analyzed by Soltis and Christiano [4]. The example considered is a simply supported W14 × 43 beam subjected to an eccentric axial force P as shown in Fig. 14. The ends of the beam are free to warp and free to rotate about X_2^G and X_3^G axes, but restrained from rotation about X_1^G axis. The translation is restrained at end point A, and is free only in the direction of X_1^G axis at points B. The geometrical and material properties are

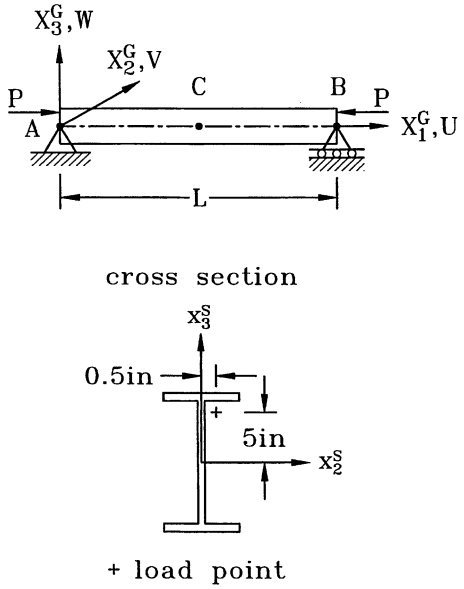

Fig. 14. Simply supported beam subjected to eccentric axial force.

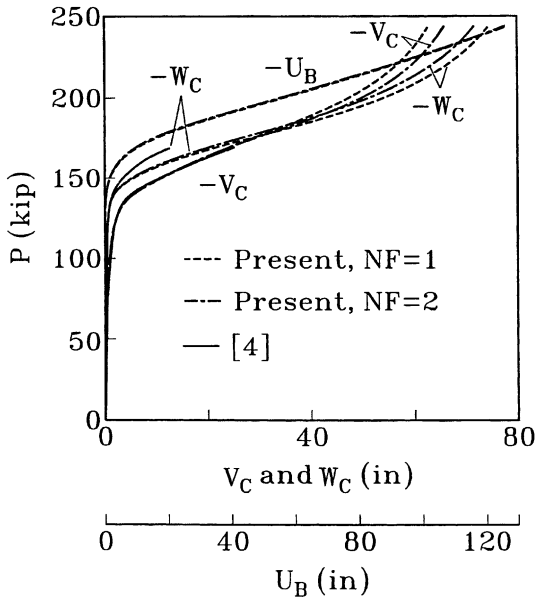

Fig. 15. Load–displacement for simply supported beam subjected to eccentric axial force.

$L = 264.6$ in., $b = 7.995$ in., $t_f = 0.53$ in., $d = 13.66$ in., $t_w = 0.305$ in., Young's modulus $E = 29,000$ ksi, and the shear modulus $G = 11,200$ ksi. The present results are obtained by using 40 elements. The buckling loads of the present study and [4] are $P_{NB} = 139.1$ and 150.1 kip, respectively. The load–deflection curves of the present study together with the results of [4] are shown in Fig. 15. As can be seen that the mid-span displacements for NF = 1 and 2 are nearly identical when the load is less than $1.3P_{NB}$. However, as the load exceeds approximately $1.4P_{NB}$, the difference between the mid-span displacements for NF = 1 and 2 is not negligible.

Example 5 (*Simply supported beam subjected to a central concentrated force*). The example considered is a simply supported I-beam subjected to a mid-span concentrated load P at the upper face as shown in Fig. 16. This example was experimentally and theoretically studied by Woolcock and Trahair [6]. The ends of the beam are free to warp and free to rotate about X_2^G and X_3^G axes, but restrained from rotation about X_1^G axis. The translation is restrained at end point A, and is free only in the direction of X_1^G axis at points B. The geometrical and material properties are $L = 143.9$ in., $b = 0.86$ in., $t_f = 0.122$ in., $h = 2.862$ in., $t_w = 0.085$ in., Young's modulus $E = 9,300,000$ psi, the shear modulus $G = 3,698,534$ psi and the self-weight is 0.0436 lb/in. The present results are obtained by using 40 elements. The results for NF = 1 and 2 are nearly identical for this example. Thus only the results for NF = 1 are given here. The present buckling load and the theoretical buckling load of [6] are 17.65 lb and 17.68 lb, respectively. The load–deflection curves of the present study together with the experimental results given in [6] are shown in Fig. 17. In Fig. 17, the initial deflections caused by the self-weight are excluded. Very good agreement between these two solutions is observed.

Example 6 (*Simply supported beam subjected to uniform moment*). The example considered is a simply supported W10 × 100 beam subjected to equal end moments M applied about its major axis as shown in Fig. 18. A disturbing moment of 0.01 M applied at the right end of the beam to initiate lateral deformations in large displacement analysis is also shown. This example was analyzed by Conci and Gattass [21] and Izzuddin [27]. The ends of the beam are free to rotate about X_2^G and X_3^G axes, but restrained from rotation about X_1^G axis. The translation is restrained at end point A, and is free only in the direction of X_1^G axis at points B. Two different warping boundary conditions are considered: (a) WF at both ends of the beam, (b) WR at both ends of the beam. Because of the rotational boundary conditions used here, the way

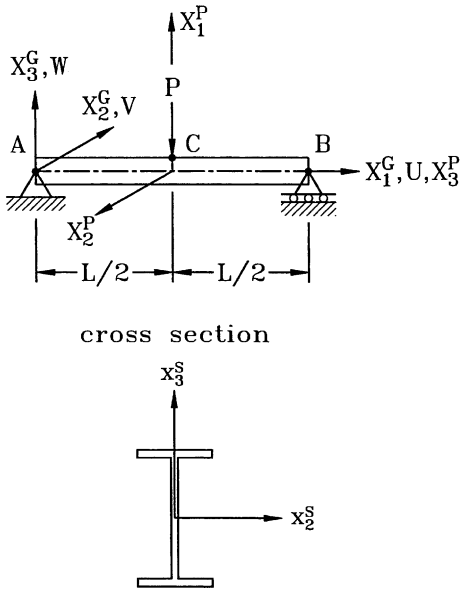

Fig. 16. Simply supported beam subjected to a central concentrated load.

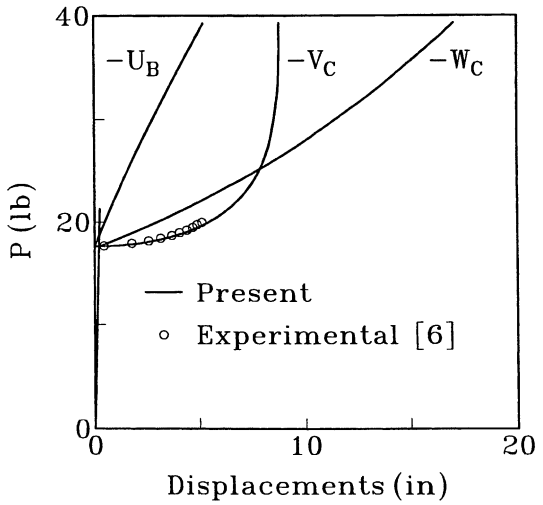

Fig. 17. Load–displacement for simply supported beam subjected to a central concentrated load.

of generating end moments is rendered irrelevant. The geometrical and material properties are $L = 610$ cm, $b = 26.2636$ cm, $t_f = 2.8448$ cm, $d = 28.194$ cm, $t_w = 1.7272$ cm, Young's modulus $E = 19,994,804$ N/ cm^2, and the shear modulus $G = 8,273,712$ N/cm^2. The theoretical buckling moments [49] are $M_{NB} = 1.7523$ and 2.4401×10^8 N/cm^2 for cases (a) and (b), respectively. The buckling moments of the present study are given in Table 2. The load–deflection curves of the present study obtained by using 40 elements together with results of [21,27] are shown in Figs. 19 and 20. As can be seen the difference between present results for NF = 1 and 2 is negligible. The present results are in good agreement with the results of [27].

Example 7 (*Cantilever angle subjected to end force*). The example considered is a cantilever right-angle frame subjected to an in-plane end force P as shown in Fig. 21. A disturbing out-of-plane load of 0.01 P applied at the free end of the frame to initiate lateral deformations in large displacement analysis is

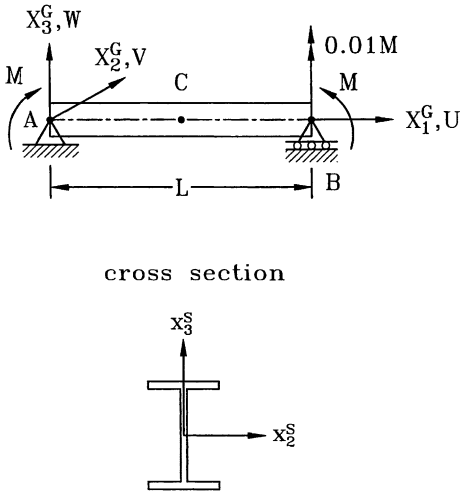

Fig. 18. Simply supported beam subjected to uniform moment.

Table 2
Buckling moment for simply supported beam subjected to uniform moment

Number of elements	M_{NB} (10^8 N/cm^2)	
	Case (a)	Case (b)
10	1.7262	2.3365
20	1.7277	2.3388
40	1.7281	2.3394
80	1.7282	2.3395

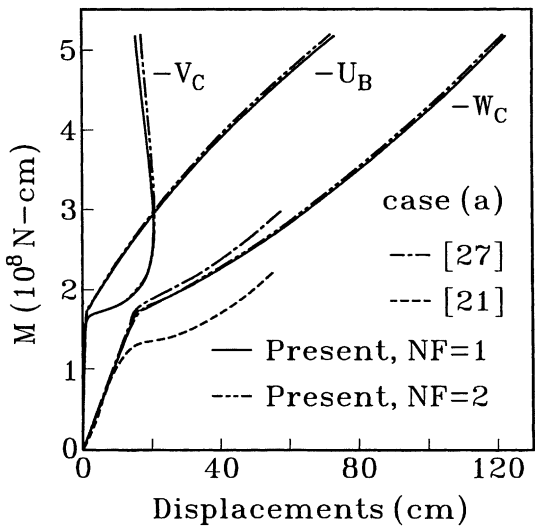

Fig. 19. Load–displacement for simply supported beam subjected to uniform moment (case a).

also shown. This example was first introduced by Yang and McGuire [15]. Each member of the frame has a W21 × 93 section with the web lying in the plane of the frame. The geometry and material properties are: $L = 240$ in.; $b = 8.42$ in.; $t_f = 0.93$ in.; $d = 21.62$ in.; $t_w = 0.58$ in.; Young's modulus

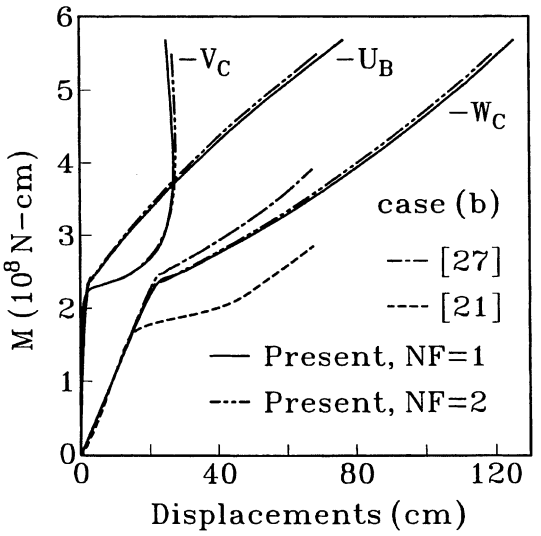

Fig. 20. Load–displacement for simply supported beam subjected to uniform moment (case b).

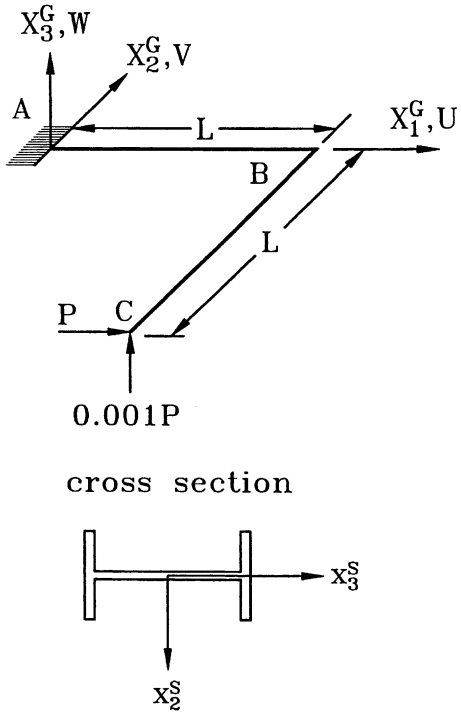

Fig. 21. Cantilever angle subjected to end force.

$E = 29,000$ ksi, and Poisson's ratio $v = 0.3$. Here, two cases are considered for the warping condition at member ends: (a) WF at the fixed end, corner joint connecting two members, and free end, (b) WR at the fixed end and corner joint, and WF at free end. The results for NF = 1 and 2 are nearly identical for this example. Thus only the results for NF = 1 are given here. The present buckling loads are $P_{NB} = 13.089$ kip and 18.679 kip, for cases (a) and (b), respectively. The corresponding linear buckling loads given in [15] are 12.33 kip and 17.42 kip, respectively. The load–deflection curves of the present study obtained by using 40 elements together with the results of [15] are shown in Figs. 22–24. As can

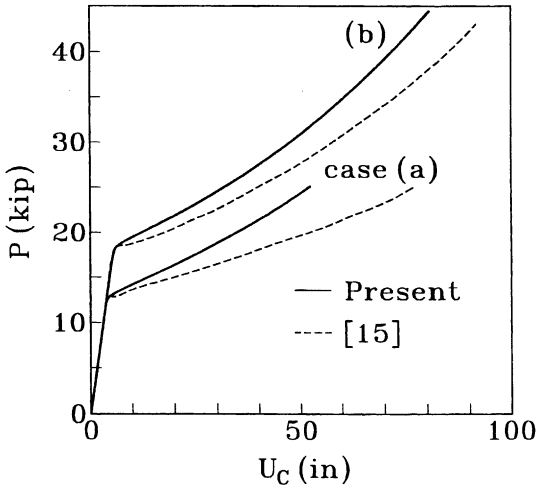

Fig. 22. Load–displacement (U) for cantilever angle subjected to end force.

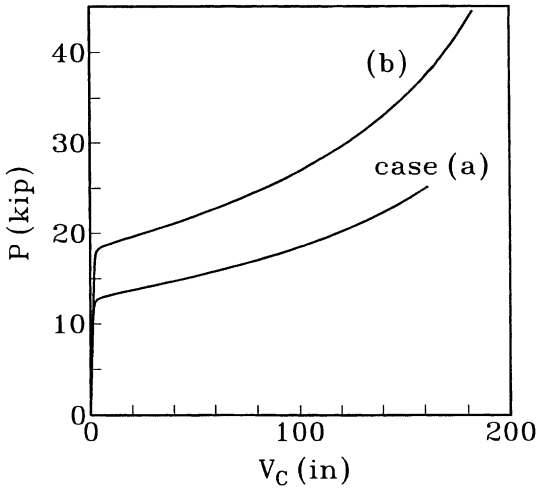

Fig. 23. Load–displacement (V) for cantilever angle subjected to end force.

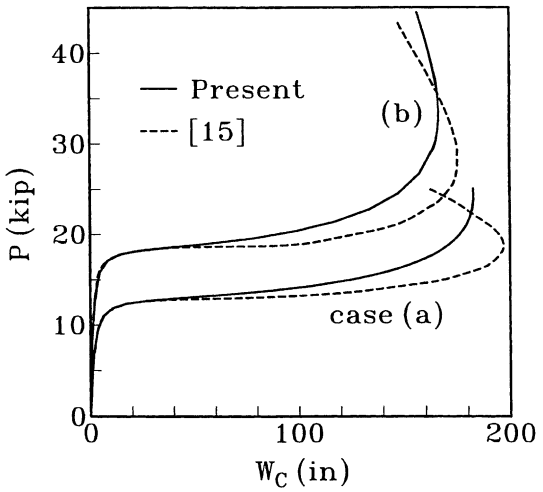

Fig. 24. Load–displacement (W) for cantilever angle subjected to end force.

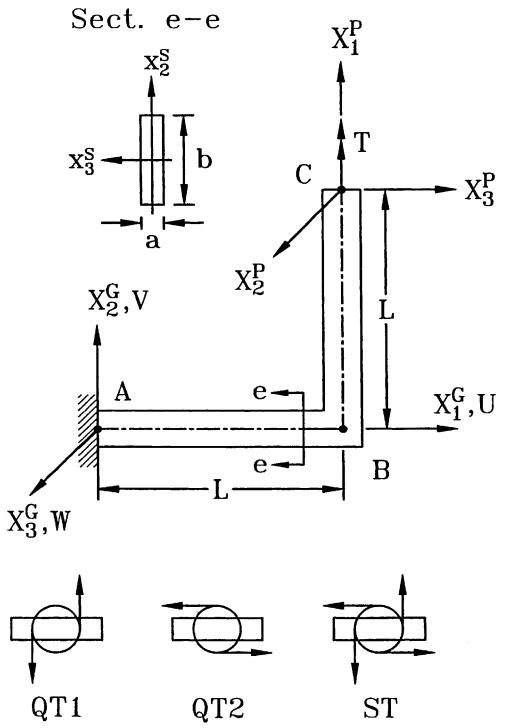

Fig. 25. Cantilever angle subjected to end torque.

Table 3
Buckling moment for cantilever angle subjected to end torsion

Type of moment	Buckling moment (N/mm^2)		
	Present	Ref. [33]	Ref. [50]
QT1	53.74	262.2	833
QT2	82.99	271.1	729
ST	104.82	274.6	1444

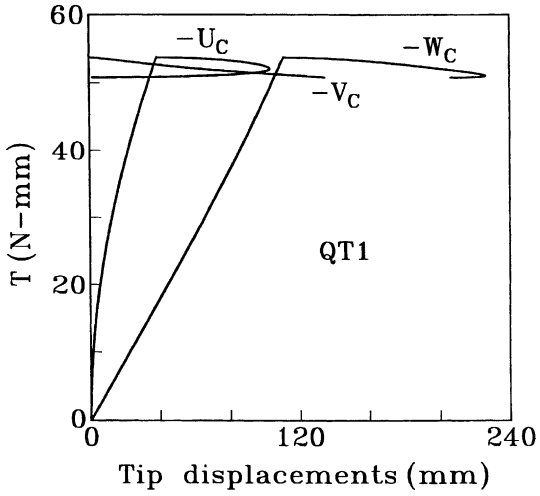

Fig. 26. Load–displacement for cantilever angle subjected to end torque (QT1).

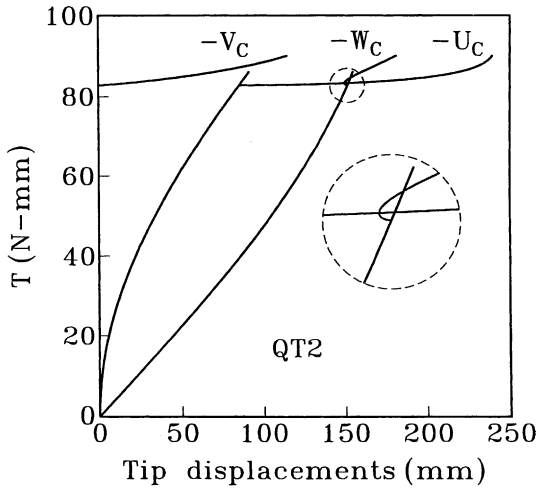

Fig. 27. Load–displacement for cantilever angle subjected to end torque (QT2).

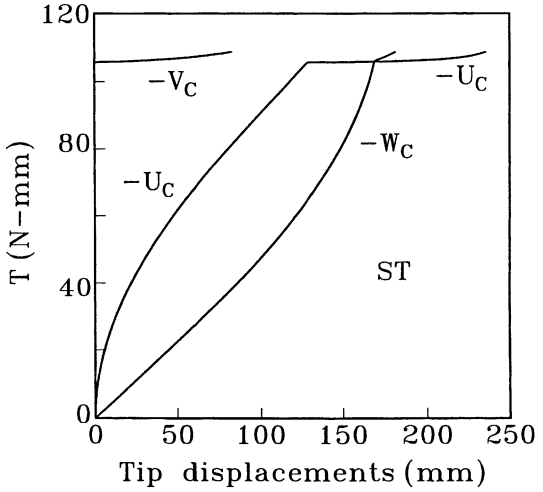

Fig. 28. Load–displacement for cantilever angle subjected to end torque (ST).

be seen the deflections of the present study and [15] are nearly identical when the load is less than P_{NB}. However, as the load exceeds P_{NB}, differences between the deflections of the present study and [15] become significant.

Example 8 (*Cantilever angle subjected to end torque*). The example considered here is a cantilever angle with rectangular cross section subjected to an end torque T. The quasitangential and semitangential moments are considered. The corresponding load base coordinates are shown in Fig. 25. The geometry and material properties of the angle are: $L = 240$ mm; $b = 0.6$ mm; $h = 10$ mm; Young's modulus $E = 71,240$ N/mm^2, and the shear modulus $G = 27,191$ N/mm^2. Here, the warping conditions at member ends are WF at the fixed end, corner joint connecting two members, and free end.

The present results are obtained by using 240 elements. The results for NF = 1 and 2 are nearly identical for this example. Thus only the results for NF = 1 are given here. The present buckling loads are shown in Table 3 together with the results of [33,50] obtained by the linear buckling analysis. As can be seen, the discrepancy between geometric nonlinear and linear buckling loads is marked. Note

that the pre-buckling displacements for this example are quite large. Thus the nonlinear buckling analysis is required for reliable buckling loads. The load–deflection curves are shown in Figs. 26–28. It can be seen that the secondary paths are unstable for QT1 moment and stable for QT2 and ST moments.

5. Conclusions

A CR TL finite element formulation of doubly symmetric thin-walled beams with open section is presented. The effects of deformation-dependent third-order terms of element nodal forces on the buckling load and post-buckling behavior are investigated. The formulations of beam elements proposed in [34,35] are modified and employed here. All coupling among bending, twisting, and stretching deformations for beam element is considered by consistent second-order linearization of the fully geometrically nonlinear beam theory. All deformation-dependent third-order terms of the element nodal forces are also considered. It is found that for most examples studied the agreement between the pre-buckling displacements and buckling loads of the present study and those given in the literature is very good. However, for some examples discrepancies between the post-buckling deflections of the present study and those given in the literature become significant. For cases with large pre-buckling displacements, the discrepancy between the nonlinear buckling loads of the present study and the linear buckling loads given in the literature is marked. The discrepancy between buckling loads and loading-deflection curves for NF = 1 and 2 is negligible for all examples studied, when the displacements and rotations are not very large. It shows that the third-order term of twist rate, $\frac{1}{2}EK_I \int \mathbf{N}'_d \theta^3_{1,s}\,\mathrm{d}s$ (Eq. (34)) is the dominant third-order term of element nodal forces. As can be seen from the results of Example 1, the effect of the third-order term of twist rate, $\frac{1}{2}EK_I \int \mathbf{N}'_d \theta^3_{1,s}\,\mathrm{d}s$ is not negligible. Thus it is suggested that when the displacements and rotations are not very large, the third-order term $\frac{1}{2}EK_I \int \mathbf{N}'_d \theta^3_{1,s}\,\mathrm{d}s$ should be retained and the rest of the third-order terms may be dropped for the geometric nonlinear analysis of thin-walled beams with open cross-section. However, when the displacements and rotations are very large, all deformation-dependent third-order terms are suggested to be retained for reliable solutions.

Acknowledgements

The authors would like to acknowledge the constructive and thoughtful comment of the referee. The research was sponsored by the National Science Council, Republic of China (Taiwan) under the contract NSC 89-2212-E-009-052.

References

[1] V.Z. Vlasov, Thin walled Elastic Beams, second ed. (English translation published for US Science Foundation by Israel Program for Scientific Translations, 1961).
[2] S.P. Timoshenko, J.M. Gere, Theory of Elastic Stability, second ed., McGraw-Hill, New York, 1963.
[3] R.S. Barsoum, R.H. Gallagher, Finite element analysis of torsional and torsional-flexural stability problems, moments, Internat. J. Numer. Methods Engrg. 2 (1970) 335–352.
[4] L.A. Soltis, P. Christiano, Finite deformation of biaxially loaded columns, J. Struct. Div. ASCE 98 (1972) 2647–2662.
[5] J.M. Anderson, N.S. Trahair, Stability of monosymmetric beams and cantilevers, J. Struct. Div. ASCE 98 (1972) 269–286.
[6] S.T. Woolcock, N.S. Trahair, Post-buckling behavior of determinate beams, J. Engrg. Mech. Div. ASCE 100 (1974) 151–171.
[7] D.O. Brush, B.O. Almroth, Buckling of Bars, Plates and Shells, McGraw-Hill, New York, 1975.
[8] H. Ziegler, Principles of Structural Stability, Birkhäuser, Basel, 1977.
[9] J.H Argyris, P.C. Dunne, D.W. Scharpf, On large displacement-small strain analysis of structures with rotation degree of freedom, Comput. Methods Appl. Mech. Engrg. 14–15 (1978) 401–451, 99–135.
[10] J.H. Argyris, O. Hilpert, G.A. Malejannakis, D.W. Scharpf, On the geometrical stiffness of a beam in space – a consistent v.w. approach, Comput. Methods Appl. Mech. Engrg. 20 (1979) 105–131.

[11] J.H. Argyris, H. Balmer, J.St. Doltsinis, P.C. Dunne, M. Haase, M. Kleiber, G.A. Malejannakis, H.P. Mlejenek, M. Muller, D.W. Scharpf, Finite element method – the natural approach, Comput. Methods Appl. Mech. Engrg. 17/18 (1979) 1–106.
[12] J.H. Argyris, S. Symeonidis, Nonlinear finite element analysis of elastic systems under nonconservative loading-natural formulation. Part I: quasistatic problems, Comput. Methods Appl. Mech. Engrg. 26 (1981) 75–123.
[13] A. Gjelsvik, The Theory of Thin Walled Bars, Wiley, New York, 1981.
[14] M.M. Attard, Lateral buckling analysis of beams by FEM, Comput. Struct. 23 (1986) 217–231.
[15] Y.B. Yang, W. McGuire, Joint rotation and geometric nonlinear analysis, J. Struct. Engrg. ASCE 112 (1986) 879–905.
[16] J.C. Simo, L. Vu-Quoc, A three-dimensional finite strain rod model. Part II: Computational aspects, Comput. Methods Appl. Mech. Engrg. 58 (1986) 79–116.
[17] W.F. Chen, E.M. Lui, Structural Stability, Theory and Implementation, Elsevier, New York, 1988.
[18] A. Cardona, M. Geradin, A beam finite element non-linear theory with finite rotations, Internat. J. Numer. Methods Engrg. 26 (1988) 2403–2438.
[19] M. Iura, S.N. Atluri, On a consistent theory and variational formulation of finitely stretched and rotated 3-D spaced-curved beams, Comput. Mech. 4 (1989) 73–88.
[20] M.A. Crisfield, A consistent co-rotational formulation for non-linear, three-dimensional, beam elements, Comput. Methods Appl. Mech. Engrg. 81 (1990) 131–150.
[21] A. Conci, M. Gattass, Natural coordinates for geometric nonlinear analysis of thin-walled frames, Internat. J. Numer. Methods Engrg. 30 (1990) 207–231.
[22] H. Chen, G.E. Blandford, Thin-walled space frames, part I: large deformation analysis theory, part II: algorithmic details and applications, J. Struct. Engrg. ASCE 117 (1991) 2499–2539.
[23] A.F. Saleeb, T.Y.P. Chang, A.S. Gendy, Effective modeling of spatial buckling of beam assemblages, accounting for warping constraints and rotation-dependency of moments, Internat. J. Numer. Methods Engrg. 33 (1992) 469–502.
[24] Y.L. Pi, N.S. Trahair, Prebuckling deflections and lateral buckling, part I: theory and part II: application, J. Struct. Engrg. ASCE 118 (1992) 2949–2985.
[25] A.S. Gendy, A.F. Saleeb, Generalized mixed finite element model for pre- and post-quasistatic buckling response of thin-walled framed structures, Internat. J. Numer. Methods Engrg. 37 (1994) 297–322.
[26] A.C.R. Djugash, V. Kalyanaraman, Nonlinear analysis of thin-walled members under biaxial bending, J. Construct. Steel Res. 31 (1994) 289–304.
[27] B.A. Izzuddin, An Eulerian approach to the large displacement analysis of thin-walled frames, Proc. Instn. Civ. Engrs. Structs. & Bldgs. 110 (1995) 50–65.
[28] G. Jelenic, M. Saje, A kinematically exact space finite strain beam model-finite element formulation by generalized virtual work principle, Comput. Methods Appl. Mech. Engrg. 120 (1995) 131–161.
[29] B.A. Izzuddin, D.L. Smith, Large-displacement analysis of elastoplastic thin-walled frames, part I: formulation and implementation and part II: verification and application, J. Struct. Engrg. ASCE 122 (1996) 905–925.
[30] L.H. Teh, M.J. Clarke, Co-rotational and Lagrangian formulations for elastic three-dimensional beam finite elements, J. Construct. Steel Res. 48 (1998) 123–144.
[31] L.H Teh, M.J. Clarke, Symmetry of tangent stiffness matrices of 3D elastic frame, J. Engrg. Mech. ASCE 125 (1999) 248–251.
[32] K.M. Hsiao, Corotational total Lagrangian formulation for three-dimensional beam element, AIAA J. 30 (1992) 797–804.
[33] K.M. Hsiao, R.T. Yang, W.Y. Lin, A consistent finite element formulation for linear buckling analysis of spatial beams, Comput. Methods Appl. Mech. Engrg. 156 (1998) 259–276.
[34] K.M. Hsiao, W.Y. Lin, A co-rotational finite element formulation for buckling and postbuckling analysis of spatial beams, Comput. Methods Appl. Mech. Engrg. 188 (2000) 567–594.
[35] K.M. Hsiao, W.Y. Lin, A co-rotational formulation for thin-walled beams with monosymmetric open section, Comput. Methods Appl. Mech. Engrg. 190 (2000) 1163–1185.
[36] J.C. Simo, L. Vu-Quoc, The role of non-linear theories in transient dynamic analysis of flexible structures, J. Sound Vib. 119 (1987) 487–508.
[37] R.D. Cook, W.C. Young, Advanced Mechanics of Materials, Macmillan, New York, 1985.
[38] H. Goldstein, Classical Mechanics, Addision-Wesley, Reading, MA, 1980.
[39] T.J. Chung, Continuum Mechanics, Prentice-Hall, Englewood Cliffs, NJ, 1988.
[40] D.J. Dawe, Matrix and Finite Element Displacement Analysis of Structures, Oxford University, New York, 1984.
[41] L.H. Teh, M.J. Clarke, New definition of conservative internal moments in space frames, J. Engrg. Mech. ASCE 123 (1997) 97–106.
[42] K.S. Schweizerhof, E. Ramm, Displacement dependent pressure loads in nonlinear finite element analysis, Comput. Struct. 18 (1984) 1099–1114.
[43] K.J. Bathe, Finite Element Procedure in Engineering Analysis, Prentice-Hall, New York, 1982.
[44] M.A. Crisfield, A fast incremental/iterative solution procedure that handles snap through, Comput. Struct. 13 (1981) 55–62.
[45] K.M. Hsiao, H.J. Horng, Y.R. Chen, A co-rotational procedure that handles large rotations of spatial beam structures, Comput. Struct. 27 (1987) 769–781.
[46] K.M. Hsiao, C.M. Tsay, A motion process for large displacement analysis of spatial frames, Internat. J. Space Struct. 6 (1991) 133–139.
[47] T. Matsui, O. Matsuoka, A new finite element scheme for instability analysis of thin shells, Internat. J. Numer. Methods Engrg. 10 (1976) 145–170.

[48] J. Chroscielewski, J. Makowski, H. Stumpf, Finite element analysis of smith, folded and multi-shell structures, Comput. Methods Appl. Mech. Engrg. 141 (1997) 1–46.
[49] A. Chajes, Principles of Structural Stability, Prentice-Hall, Englewood Cliffs, NJ, 1974.
[50] Y.B. Yang, S.R. Kuo, Buckling of frames under various torsional loading, J. Engrg. Mech. ASCE 117 (1991) 1681–1697.